JACS
JOURNAL OF THE AMERICAN CHEMICAL SOCIETY
pubs.acs.org/JACS
Article

Design and Synthesis of Kekulè and Non-Kekulè Diradicaloids via the Radical Periannulation Strategy: The Power of Seven Clar's Sextets

Febin Kuriakose, Michael Commodore, Chaowei Hu, Catherine J. Fabiano, Debashis Sen, Run R. Li, Shubham Bisht, Ökten Üngör, Xinsong Lin, Geoffrey F. Strouse, A. Eugene DePrince, III, Robert A. Lazenby, Frederic Mentink-Vigier, Michael Shatruk, and Igor V. Alabugin*

Cite This: J. Am. Chem. Soc. 2022, 144, 23448−23464
Read Online
ACCESS | Metrics & More | Article Recommendations | Supporting Information

ABSTRACT: This work introduces an approach to uncoupling electrons via maximum utilization of localized aromatic units, i.e., the Clar's π-sextets. To illustrate the utility of this concept to the design of Kekulé diradicaloids, we have synthesized a tridecacyclic polyaromatic system where a gain of five Clar's sextets in the open-shell form overcomes electron pairing and leads to the emergence of a high degree of diradical character. According to unrestricted symmetry-broken UCAM-B3LYP calculations, the singlet diradical character in this core system is characterized by the y_0 value of 0.98 (y_0 = 0 for a closed-shell molecule, y_0 = 1 for pure diradical). The efficiency of the new design strategy was evaluated by comparing the Kekulé system with an isomeric non-Kekulé diradical of identical size, i.e., a system where the radical centers cannot couple via resonance. The calculated singlet−triplet gap, i.e., the ΔE_{ST} values, in both of these systems approaches zero: −0.3 kcal/mol for the Kekulé and +0.2 kcal/mol for the non-Kekulé diradicaloids. The target isomeric Kekulé and non-Kekulé systems were assembled using a sequence of radical periannulations, cross-coupling, and C−H activation. The diradicals are kinetically stabilized by six *tert*-butyl substituents and (triisopropylsilyl)acetylene groups. Both molecules are NMR-inactive but electron paramagnetic resonance (EPR)-active at room temperature. Cyclic voltammetry revealed quasi-reversible oxidation and reduction processes, consistent with the presence of two nearly degenerate partially occupied molecular orbitals. The experimentally measured ΔE_{ST} value of −0.14 kcal/mol confirms that **K** is, indeed, a nearly perfect singlet diradical.

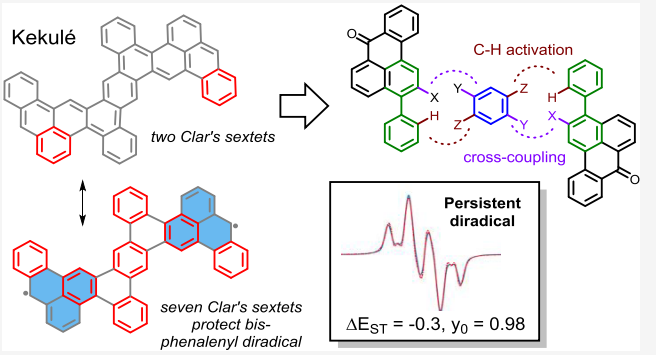

INTRODUCTION

Due to the presence of singly occupied nonbonding molecular orbitals (MOs), open-shell polycyclic aromatic hydrocarbons (PAHs) display unique optical, electronic, and magnetic properties.[1−7] PAHs that possess two unpaired electrons at two low-energy singly occupied nonbonding MOs can be described as diradicaloids. The degree of coupling between these electrons determines relative contributions of the closed-shell form and the open-shell form to the overall electronic structure and defines the singlet−triplet (S−T) gap, ΔE_{ST}.[8] These electronic features can lead to enhanced polarizability and impressive third-order nonlinear optical properties.[9−13] The electronic nature of open-shell diradicaloids also lends itself for the development of the singlet fission processes that can increase the efficiency of future photovoltaic devices.[14−19]

The two conceptually different approaches to conjugated diradicals are based on Kekulé vs non-Kekulé structures (Figure 1). The non-Kekulé structures have open-shell character because of their intrinsic bonding pattern that prevents the radical centers from coupling via resonance. In contrast, the open-shell character in the Kekulé diradicals is

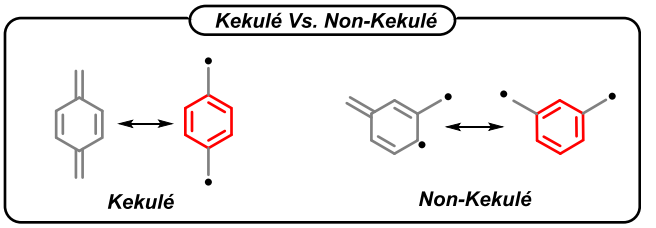

Figure 1. Kekulé vs non-Kekulé diradicals.

Received: September 10, 2022
Published: December 14, 2022

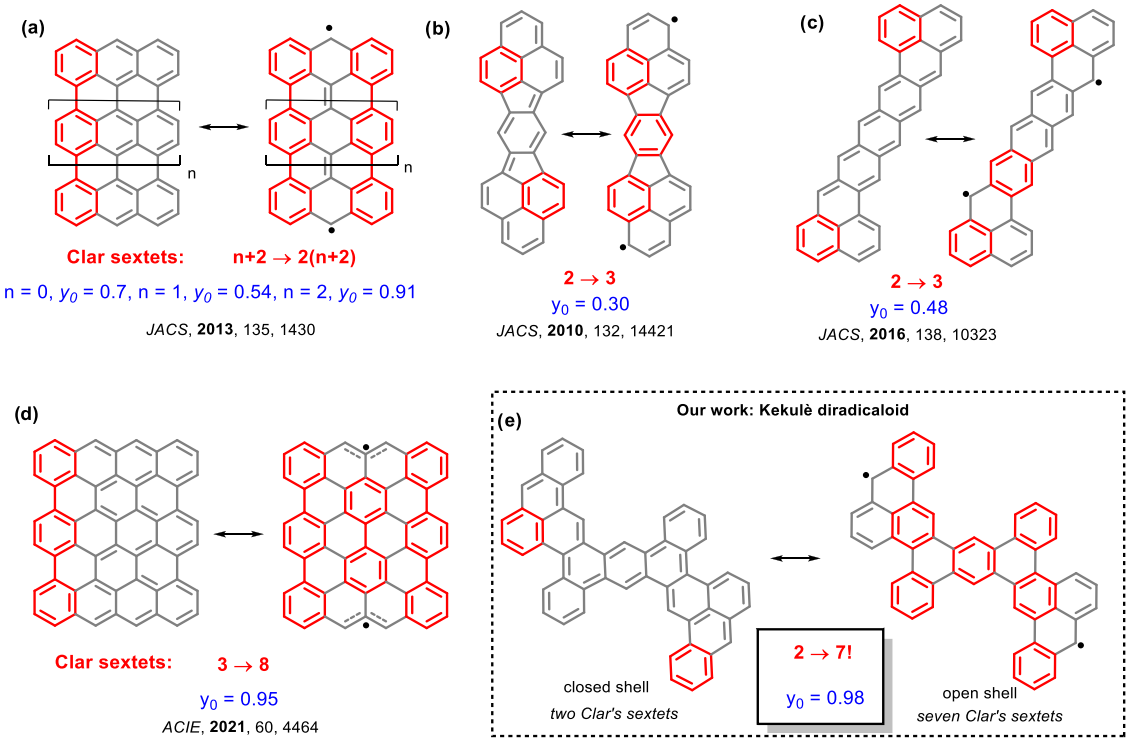

Figure 2. Literature designs of Kekulé diradicaloids: (a) perifused acenes, (b) bisphenalenyl, (c) nonazethrene, (d) [4,3]periacene with high diradical character, and (e) our design.

only generated when the open-shell diradical resonance structure can overcome the "classic" closed-shell preference due to a combination of sufficiently strong electronic factors.

The challenge for making Kekulé diradicals is that the two radical centers formally originate from uncoupling of two paired electrons, i.e., the effective loss of one chemical bond. For the same reasons, why the formation of chemical bonds is inherently favorable and can be considered as a cornerstone of molecular science, losing a chemical bond to form a diradical is inherently unfavorable. Although uncoupling electrons in a π-bond come with a smaller penalty than breaking a σ-bond, the penalty is still significant as one can glimpse from the ~58 kcal/mol energy difference between the ground state and the triplet state of ethylene (i.e, the singlet/triplet (S/T) gap[20]). This penalty for losing a bond can be decreased by additional factors that favor the diradical form, e.g., extended conjugation,[21,22] gain of aromatic stabilization,[23−25] loss of antiaromaticity,[26−32] etc.

In this work, we will concentrate on using localized aromaticity, i.e., the Clar's π-sextets to uncouple electrons in a π bond. The Clar's rule is one of the key ideas of general importance in the chemistry of PAHs. This rule states that the Kekulé resonance structure with the largest number of disjoint benzene-like aromatic π-sextets, i.e., "the Clar's sextets", contribute the most to the PAH properties. The larger number of Clar's sextets in one of the isomeric PAHs usually predicts its greater stability.[33−37]

Recent research has focused on Kekulé diradicaloids with a variety of edge structures such as perifused acenes,[38−42] bisphenalenyls,[43−45] zethrenes,[46−49] and quinoidal rylenes[50−52] (Figure 2). Although these structures are inherently unstable, chemical modifications with bulky groups and electron-withdrawing groups can provide varying degrees of kinetic protection. The degree of diradical character in singlet diradicaloids can be described by the diradical index y_0, which ranges from y_0 = 1 (pure diradical) to y_0 = 0 (pure closed shell).[53,54] Very recently, Chi and co-workers reported a kinetically stable [4,3]periacene diradicaloid with a large diradical character of y_0 = 0.94. The observed high diradical character can be attributed to the aromatic stabilization originating from the gain of five additional Clar's sextets in the open-shell form.[55,56]

Guided by the idea that high diradical character can be deduced qualitatively from Clar's rule and that gaining additional Clar's sextets in the open-shell form is the key to obtaining a stable ground-state singlet diradicaloid with higher diradical character, we have considered a relatively simple, yet unknown, system shown in Figure 2e where the diradical formation is assisted by the occurrence of seven (7) Clar sextets. This polycyclic framework includes part of the "ideal" system for the design of diradicals that we will discuss below.

RESULTS AND DISCUSSION

Rational Design of Polyaromatic Diradicals. The new design reported in this work originated from the question to what extent can one exploit the Clar's rule for the systematic search of molecules with high diradical character. The starting point is the idea that making the singlet diradicaloid electronically stable while having high degree of diradical character is facilitated by gaining the maximum number of Clar's aromatic sextets in the open-shell form. Based on this idea, we propose a general approach to the design of novel diradicaloids in the following way. The starting point is simple—choose a system with the maximum number of Clar's sextets ("fully benzenoid" in Clar's terms[56]) for a given ring system, add CH_2 radicals, and explore the electron pairing topology. This is a systematic approach to interesting Kekulé and non-Kekulé diradicaloid topologies, which have not been

https://doi.org/10.1021/jacs.2c09637
J. Am. Chem. Soc. 2022, 144, 23448−23464

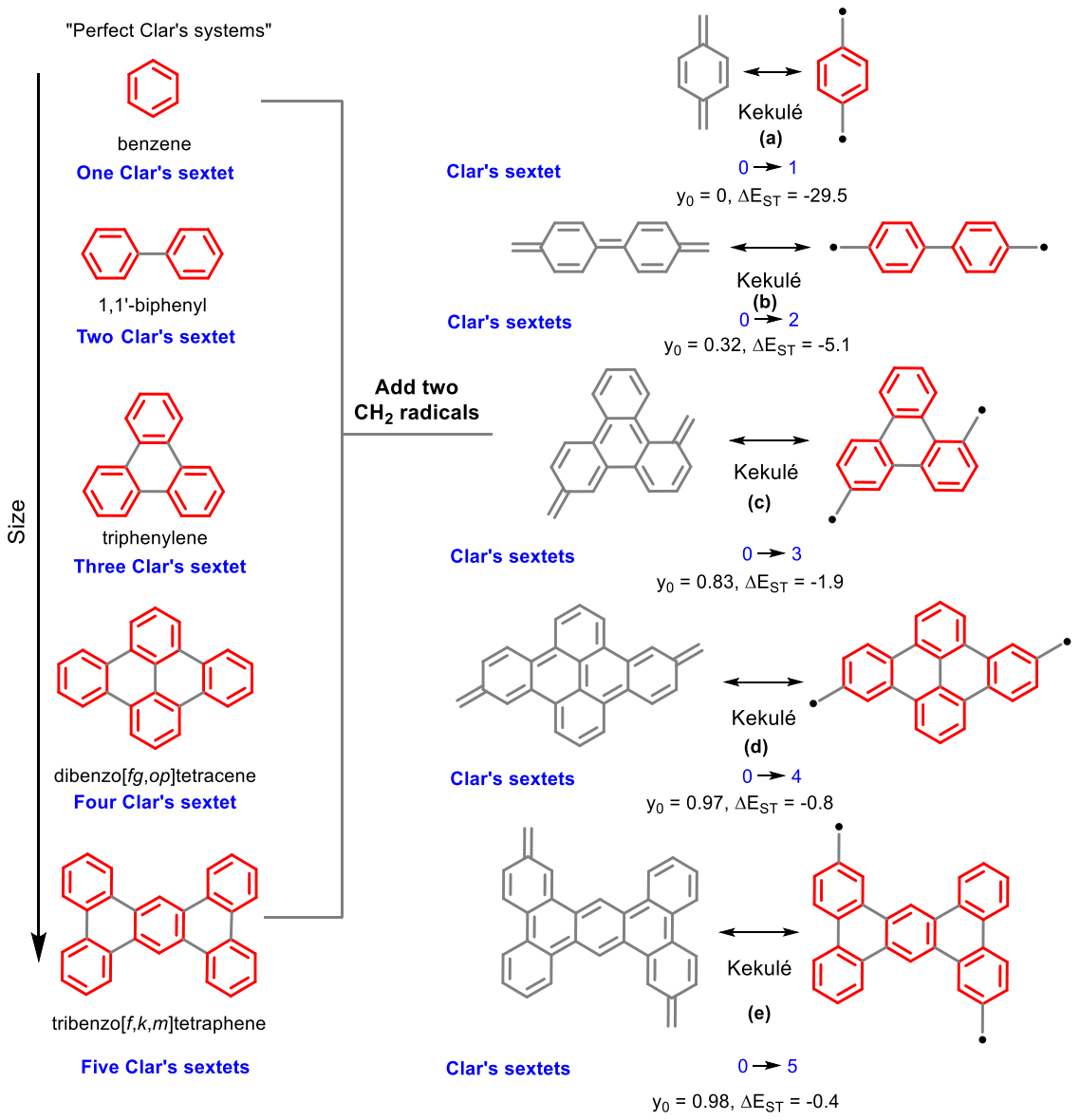

Figure 3. Introduction of diradical character into Kekulé polyaromatic systems based on the "ideal" systems with the maximum number of Clar's sextets is facilitated in the larger systems. Calculations are performed at (U)CAM-B3LYP/6-31G(d,p) level of theory. See the Supporting Information (SI) for the full list of possibilities.

explored previously. We give a full list of these diradicals in Figure S5 and only give the illustrative examples and a summary below.

To start, let us add two para-CH_2 radicals to benzene. The resulting molecule has a quinoid ground state. Transforming it into a diradical would create only one Clar's sextet. Hence, the S/T gap is relatively large (~30 kcal/mol) and the y_0 parameter of 0 indicates no diradical character. However, progressive expansion of the core to biphenyl (Tschitschibabin's hydrocarbon[57]), triphenylene, dibenzo[*fg*,*op*]tetracene, and tribenzo[*f*,*k*,*m*]tetraphene gradually changes the situation. Use of these cores allows one to gradually increase the number of Clar's sextets gained upon conversion of quinoid structures to the diradical counterparts (two, three, four, and five additional Clar's sextets, respectively). Note the rapid decrease in the respective S/T gaps (5.1 > 1.9 > 0.8 > 0.4) and the concomitant increase in the y_0 value (0.32 < 0.83 < 0.97 < 0.98) (Figure 3).

The number of possibilities is large because the CH_2 "units" can be attached to the "ideal" polyaromatic cores in a variety of patterns. These patterns also include systems that are inherently incapable of electron pairing due to their topology. Such systems correspond to non-Kekulé structures. For example, adding two methylene radicals to triphenylene yielded a total of 16 unique results with ten Kekulé and six non-Kekulé structures (see Figure S5). For dibenzo[*fg*,*op*]-tetracene, there are 27 choices for appending two methylene radicals, 15 of which are Kekulé and 12 are non-Kekulé. For tribenzo[*f*,*k*,*m*]tetraphene, PAH with the most number of Clar's sextets for a seven-ring system, the process creates 45 different molecular systems—25 Kekulé and 20 non-Kekulé (Figure S6). This discussion illustrates the large amount of potential diradicals available when starting with the privileged polyaromatic cores with the maximum number of Clar's sextets.

https://doi.org/10.1021/jacs.2c09637
J. Am. Chem. Soc. 2022, 144, 23448−23464

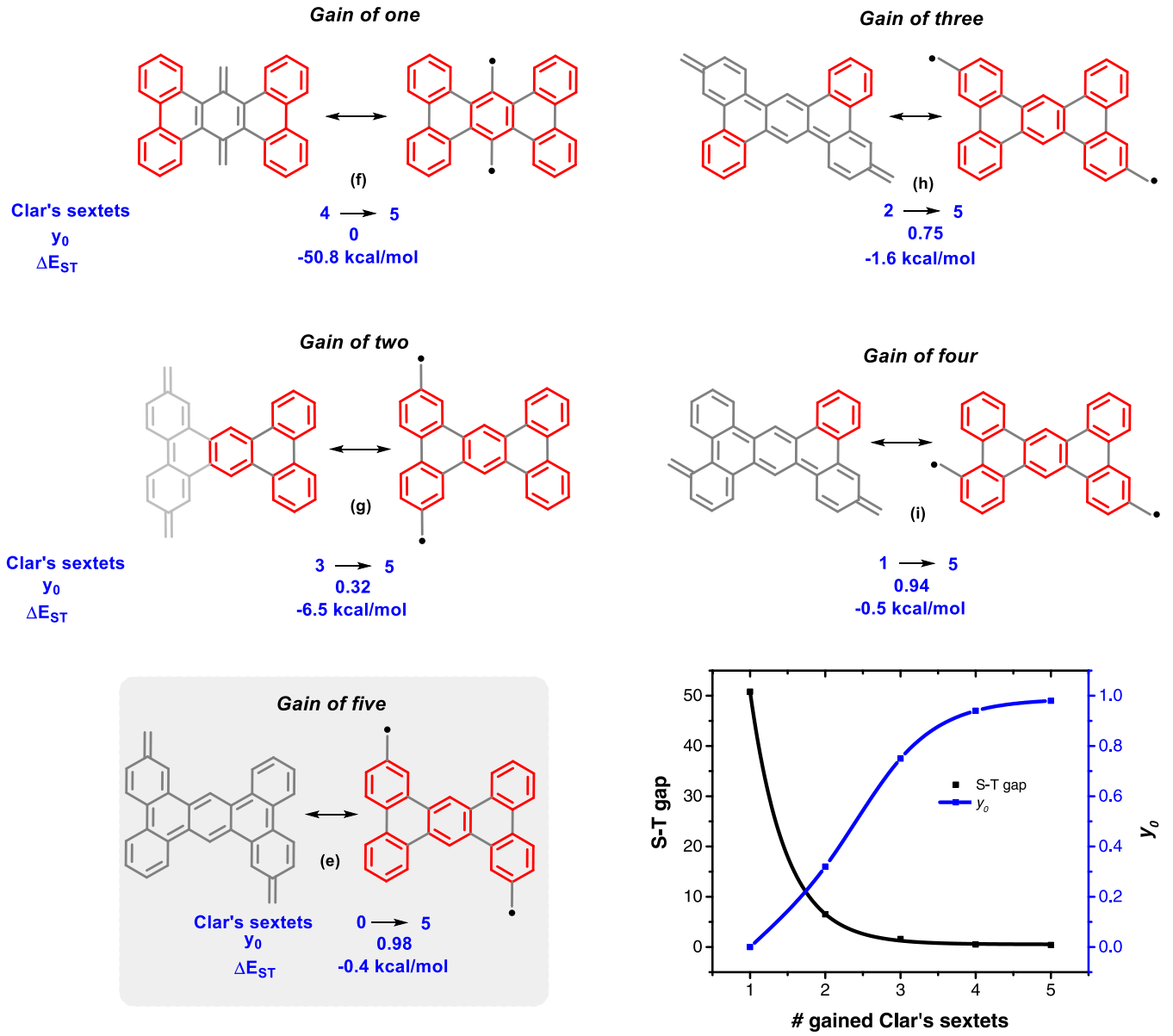

Figure 4. Selected diradicals built upon the tribenzo[*f*,*k*,*m*]tetraphene core. Not all of the patterns based on "ideal Clar's systems" are equal: the gain of Clar's sextets in the diradical form varies depending on the relative placement of the spin centers. Bottom right: the S/T gap as a function of the number of gained Clar's sextets. Calculations are performed at (U)CAM-B3LYP/6-31G(d,p) level of theory.

However, not all of these systems are equal as some of them do not lose all of their Clar's sextets upon electron pairing. Their contribution of diradical character depends greatly on the relative placement of the two spin centers. Based on the location of spin centers, these molecules can gain one, two, three, four, or five Clar's sextets in the open shell. In fact, only a few of the 45 possibilities for the tribenzo[*f*,*k*,*m*]tetraphene show the maximum gain in the local Clar's aromaticity (see the SI Section for the full list). Computational analysis on the effect of the number of gained Clar's sextets on the diradical character and singlet−triplet gap (Figure 4) found, as expected, that the structures with the greatest gain have the most diradical character. Overall, the S/T gap decreases exponentially with the increase in the number of gained Clar's sextets in the open-shell form.

Figure 4 illustrates it quite clearly. Only one Clar's sextet is gained in compound **f** that has a closed-shell ground state with zero diradical character and a high singlet−triplet gap of −51 kcal/mol. Gain of two Clar's sextets in the isomer **g** introduces a nonzero diradical character of $y_0 = 0.32$ and the much lower S/T gap of −6.5 kcal/mol. As the gain in Clar's sextets increases, the degree of diradical character y_0 increases ($0 < 0.32 < 0.75 < 0.94 < 0.98$) and the singlet−triplet gap decreases ($50.8 > 6.5 > 1.6 > 0.5 > 0.4$). The open-shell form of the bottom structure **e** gains maximum (five) Clar's sextets. As expected, this results in a very high diradical character, $y_0 = 0.98$, and very small singlet−triplet gap, $\Delta E_{ST} = -0.4$ kcal/mol (Figure 4). This is the system that was chosen for the experimental pursuit.

Furthermore, one can expand the "ideal systems" by a number of additional design elements such as conjugating side chains or fused rings as illustrated in Figure 5. The parent system with the two methylene radicals (the Kekulé diradical **e**) already has high diradical character of $y_0 = 0.98$ and S−T gap of −0.4 kcal/mol. Extending conjugation at the radical centers, e.g., by adding either a double bond or a benzene ring,

https://doi.org/10.1021/jacs.2c09637
J. Am. Chem. Soc. 2022, 144, 23448−23464

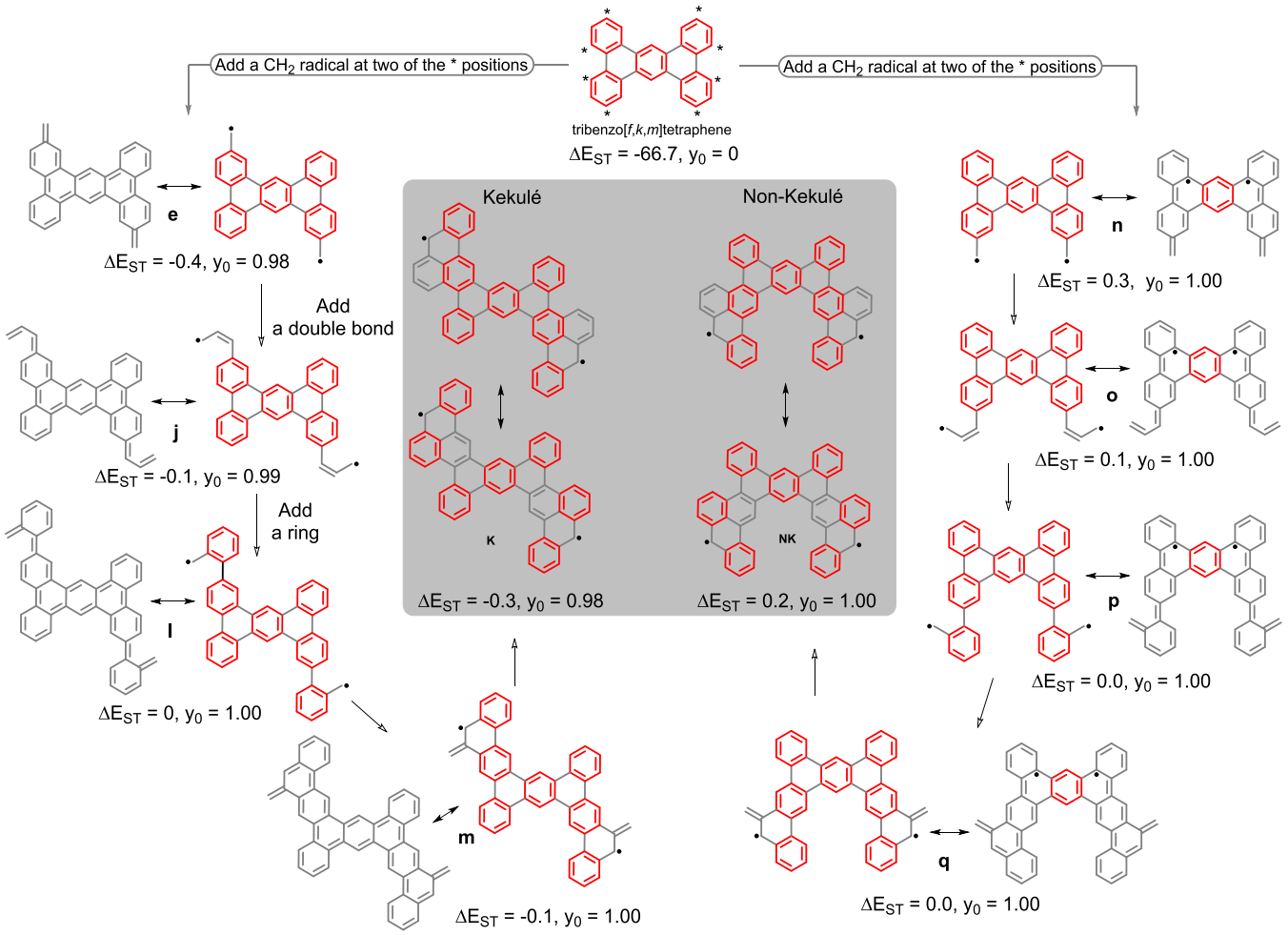

Figure 5. Extending the parent tribenzo[*f*,*k*,*m*]tetraphene framework to our Kekulé and non-Kekulé system. Calculations are performed at (U)CAM-B3LYP/6-31G(d,p) level of theory.

can further stabilize the radicals. By adding two phenyl rings, one can amplify the effect even more. This change increases the diradical character to $y_0 = 1.00$ for **l** and decreases the S−T gap of **l** to zero. The nearly perfect diradical character can be explained by the gain of seven Clar's sextets in the open-shell form relative to the closed-shell configuration with zero Clar's sextets. Interestingly, **p** and **l** have one Clar's sextet more than tribenzo[*f*,*k*,*m*]tetraphene. By following this diradical evolution process, we have reached a point where we made two perfect diradicals, one Kekulé and one non-Kekulé, i.e., **p** and **l**. Now, the question is what are the practically accessible versions of these systems? One can extend the pattern to cyclic diradicals **m** and **q**, but still has a resonance structure where the radical center is outside the cycle. If we fuse an additional cycle at this position, we reach our target fully cyclic Kekulé, **K**, and non-Kekulé, **NK**, structures where a high degree of diradical character is preserved (center of Figure 5).

Non-Kekulé Alternatives. As one can see from Figure 5 and the SI, this general design concept also offers a number of non-Kekulé diradicals. One of the non-Kekulé structures that is close structurally to the target Kekulé radical is highlighted in the right part of Figure 5. We thought that this parallel design can provide a valuable opportunity to compare the two types of diradicals side-by-side. Non-Kekulé diradicaloids have a high-spin (triplet) ground state that makes them reactive and renders their solution synthesis challenging. One of the most studied non-Kekulé diradicaloids is triangulene (Clar's hydrocarbon) that is the smallest triplet ground-state PAH. Most of the initial solution-based synthesis of triangulene resulted in polymerization of the formed diradicaloid.[58,59] The triplet ground state of triangulene was confirmed by Nakasuji and co-workers where they made 2,6,10-tri-*tert*-butyltriangulene.[60] However, since the *tert*-butyl groups were not placed at positions of highest spin density, the compound easily got polymerized. Recently, Gross and co-workers reported an on-surface synthesis of unsubstituted triangulene. A combination of scanning tunneling and atomic force microscopy (STM/AFM) was used to dehydrogenate the precursor molecules to get the product triangulene.[61] Arikawa et al. reported the solution synthesis and isolation of crystalline triangulene. The introduction of bulky substituents to the reactive zigzag edges helps to kinetically stabilize the diradical, and the triplet ground state was confirmed by electron paramagnetic resonance (EPR) studies.[62] Wu and co-workers reported first persistent triplet diradicaloid, 1,14:11,12-dibenzopentacene in solution. The persistence of this triplet diradicaloid below −78 °C was ascribed to the kinetic blocking of most reactive sites and to a large extent of spin delocalization in the molecular framework. Although the triplet ground state was confirmed by ESR measurements, the compound was stable in solution only under −78 °C and inert atmosphere.[63] So, the search for stable non-Kekulé diradicaloids continues (Figure 6). Very recently,

https://doi.org/10.1021/jacs.2c09637
J. Am. Chem. Soc. 2022, 144, 23448−23464

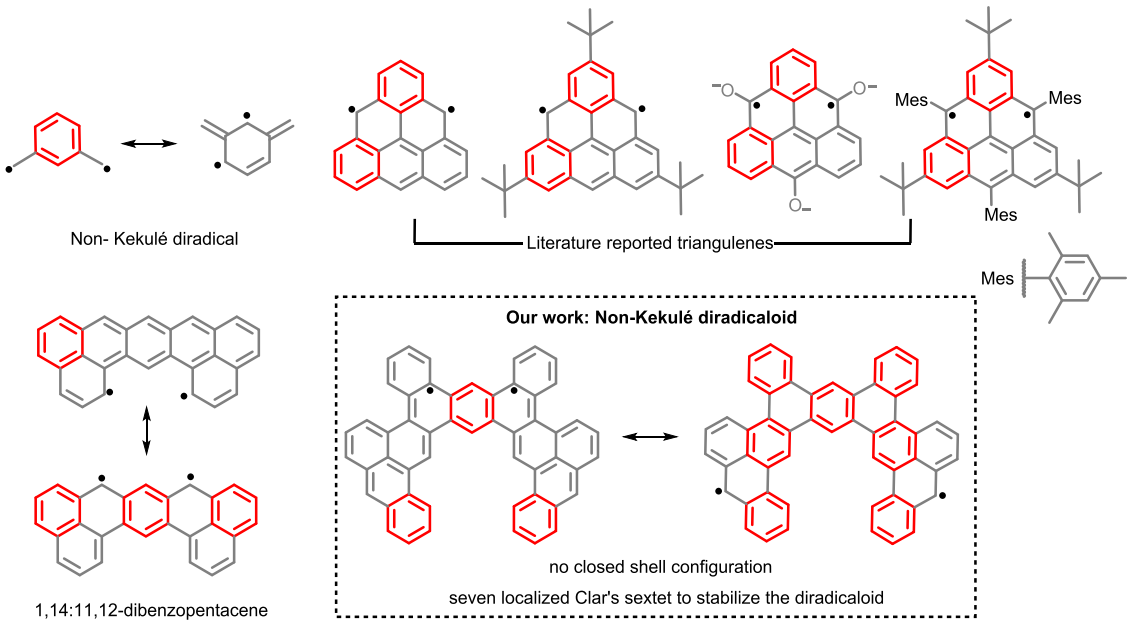

Figure 6. Various non-Kekulé structures from the literature in comparison to the system presented in our work.

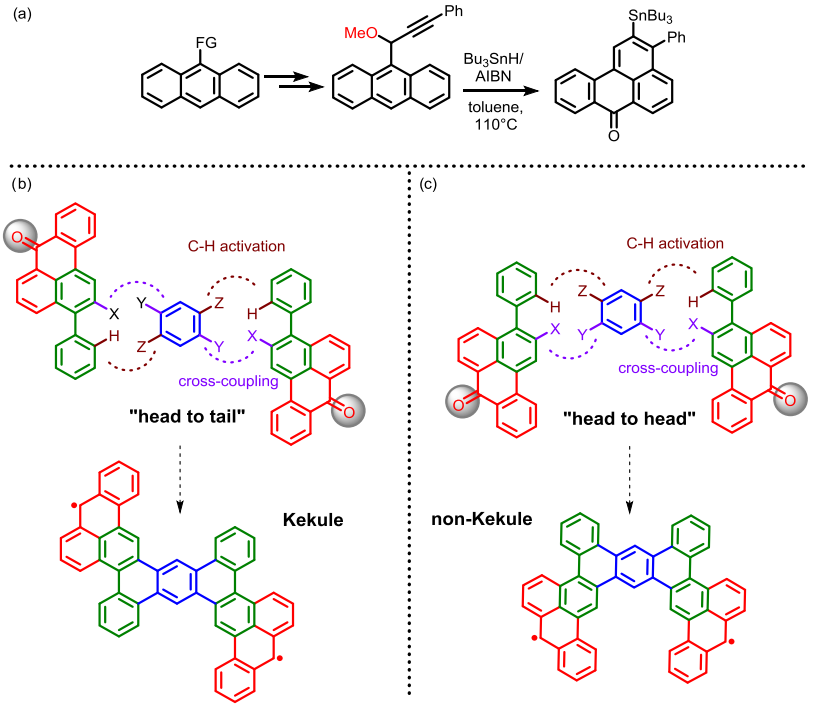

Figure 7. (a) General scheme for periannulations. (b, c) Synthetic design of diradicaloids.

Jurič̆ek and co-workers reported that trimesityltriangulene is persistent,[64] while the groups of Wu[65] and Rajca[66] reported high-spin nitrogen-doped nanographenes.

Advantages of *Peri*-annulations. Synthesis of extended polyaromatics often provides interesting synthetic challenges that span innovation.[67−94] In the present case, an attractive synthetic route to diradicaloids is opened by our recent work on radical alkyne periannulations (i.e., "zigzag annulations")[95−97] where we developed a new strategy for expanding the scope of π-annulations at the zigzag edge of PAHs (Figure 7a). Fortuitously, the pericyclizations provide the necessary pieces for accomplishing the synthesis of new diradicals in a concise and modular fashion. In particular, this reaction provides functionalized benzanthrones that can be considered as masked phenalenyl radicals with an extra localized Clar's sextet. These pieces can be fused, like Legos, into larger structures where, by changing the starting materials, we can control the associated characteristics and properties and fine-tune the properties of diradical graphene fragments. For example, if the two benzanthrone units are connected in a head-to-tail fashion using a phenyl linker by a sequence of cross-coupling and C−H activation steps, the resulting system can be converted into a Kekulé diradicaloid. The resulting Kekulé diradicaloid will be electronically stabilized in the open-

https://doi.org/10.1021/jacs.2c09637
J. Am. Chem. Soc. 2022, 144, 23448−23464

Scheme 1. Synthesis[a]

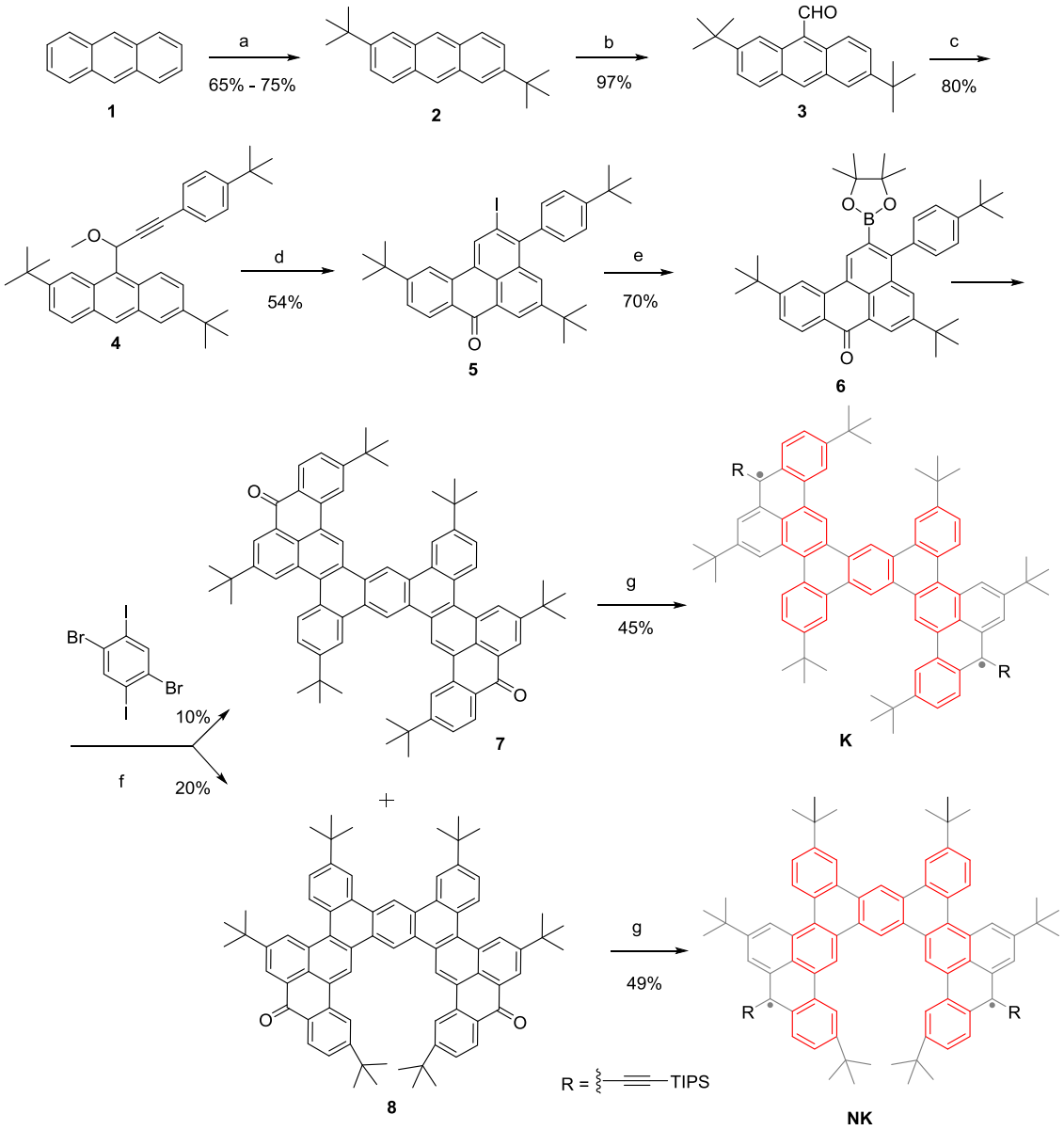

[a](a) *t*BuOH, trifluoroacetic acid (TFA), reflux, 16 h; (b) $CHCl_2OMe$, $TiCl_4$, dichloromethane (DCM), 0 °C to reflux, 1 h; (c) (1) *tert*-ButylPhCCH, *n*-BuLi, tetrahydrofuran (THF), −78 °C to room temperature (rt), 3 h and (2) MeI, rt, 12 h; (d) (1) Bu_3SnH (2 equiv), azobisisobutyronitrile (AIBN) (1 equiv) toluene, 110 °C, 18 h; (2) I_2, DCM, rt, 2 h; and (3) 2,3-dichloro-5,6-dicyano-1,4-benzoquinone (DDQ), DCM, rt, 2 h; (e) bis(pinacolato)diboron, $Pd(dppf)Cl_2$, dimethylformamide (DMF), KOAc, 80 °C, 6 h; (f) (1) $Pd(PPh_3)_4$ (0.2 equiv), K_2CO_3 (5 equiv), 18-crown-6 (0.2 equiv), toluene/H_2O (4:1), 100 °C, 18 h and (2) $Pd(PCy_3)_2Cl_2$ (0.2 equiv), pivalic acid (0.2 equiv), Cs_2CO_3 (5 equiv), reflux, 20 h; (g) (1) TIPSCCH, *n*-BuLi, THF, −78 °C to rt and (2) $SnCl_2$, 0 °C to rt.

shell configuration by seven localized Clar's aromatic sextets as opposed to two Clar's sextets in the closed-shell configuration (Figure 7b). On the other hand, connecting the two benzanthrone units in a head-to-head fashion creates the non-Kekulé diradicaloid. The latter is also stabilized by seven localized Clar's sextets but lacks a spin-paired closed-shell resonance structure (Figure 7c).

Herein, we report a Kekulé diradicaloid with a high diradical character (0.98) and reasonable kinetic stability (half-lifetime ∼ 42 h) and compare its properties with an isomeric non-Kekulé diradicaloid with a half-lifetime of 2 h. This comparison shows that a Kekulé structure, where electron pairing is possible, can with the help of Clar's sextets rival the analogous non-Kekulé structure in the degree of diradical character and stability.

Synthesis. The synthesis started with the introduction of *tert*-butyl groups to anthracene to yield 2,6-di-*tert*-butylanthracene, **2**, to increase the solubility and kinetic stability of the polyaromatic target products (Scheme 1). Formylation at the ninth position of 2,6-di-*tert*-butylanthracene yielded compound **3** in high yield. Addition of 4-*tert*-butylphenyl acetylide to 2,6-di-*tert*-butylanthracene-9-carbaldehyde, followed by in situ reaction with methyl iodide, gives the propargylic ether precursor **4** for the radical cyclization in 80% yield. The iodo-substituted benzanthrone product **5** is formed in the overall 54% yield after the subsequent Bu_3Sn-mediated radical

https://doi.org/10.1021/jacs.2c09637
J. Am. Chem. Soc. 2022, 144, 23448−23464

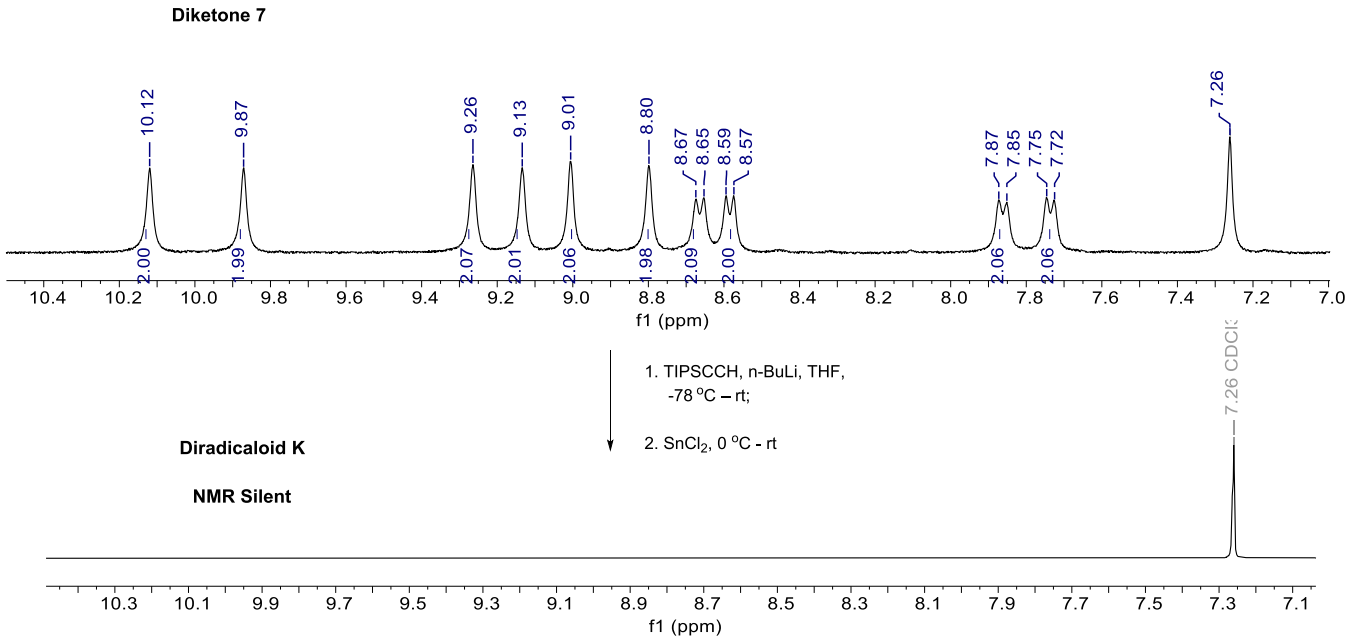

Figure 8. Comparison of ^{1}H NMR spectra of diradicaloid **K** and its precursor diketone **7**.

cyclization, iodination, and oxidation. The cyclization is the key step that enabled us to get functionalized precursors for the following assembly of the final polyaromatic system. Borylation of compound **5** yielded **6** in 70% yield.

Compound **6** is subjected to the one-pot Pd-catalyzed Suzuki coupling and dehydrohalogenation sequence with 1,4-dibromo-2,5-diiodobenzene to form the mixture of the two target polyaromatic diketones **7** and **8** in 10 and 20% isolated yields, respectively. Although formation of the Kekulé precursor can be rationalized by the sequence of Suzuki reaction at the iodo-substituted positions and C−H/C−Br coupling, the formation of isomeric head-to-head dimer suggests that the mechanistic picture is likely to be more interesting and complex. Although the reaction mechanism is not clear, one can speculate that it involves a benzyne intermediate (Scheme S1).

Due to the presence of six *tert*-butyl groups attached to the core, the diketones are soluble in various organic solvents and could be crystallized to provide suitable samples for X-ray crystallography. The *tert*-butyl groups also serve as a steric bulk to stabilize the final diradicaloids. Subsequent addition of TIPS-acetylide and reduction with $SnCl_2$ provided fully deoxygenated polyaromatic diradicaloids "Kekulé" (**K**) and "non-Kekulé" (**NK**) in moderate yields.

Both diradicaloids **K** and **NK** are purified on a silica gel column deactivated by triethylamine. **K** has a reasonably long half-lifetime of 42 h in dichloromethane (DCM) under ambient air and light. Interestingly, its triplet counterpart, **NK**, has a noticeably shorter lifetime of 2 h in DCM under ambient light and air. Both **K** and **NK** are NMR silent at room temperature, which is consistent with their paramagnetic character (Figure 8).

Crystal Structure. Although we have been unable to obtain single crystals of both **K** and **NK** due to intrinsic instability of these diradicaloids, we carried out crystallographic analysis on single crystals of the precursor diketones **7** and **8** that were grown by slow diffusion of methanol into a dichloromethane solution of **7** or **8**. Compound **7** crystallizes in a monoclinic space group $P2_1/c$, with the asymmetric unit containing one and a half molecule of **7** and one interstitial dichloromethane molecule (Figure 9a). Fitting a least-square plane only through 52 cyclic C atoms of each [4]helicene shows that one of the molecules is substantially more distorted from planarity than the other, with the sums of squared atom-to-plane distances equal to 32.6 and 12.9 Å^2 and the corresponding distances varying from −1.037 to 1.843 Å and from −1.016 to +1.016 Å, respectively (the negative and positive signs indicate atoms arranged on opposite sides of the plane). In the less distorted [4]helicene, the two halves of the molecule are related by a crystallographic inversion center. Examination of the crystal packing reveals extensive intermolecular $\pi-\pi$ interactions that result in chains of molecules along the *a*-axis (Figure 9b). The interactions between these chains are relatively weaker.

Compound **8** crystallizes in an orthorhombic space group *Pbca*. The asymmetric unit contains only one [4]helicene molecule (Figure 9c). Steric repulsion between the terminal *tert*-butyl groups in **8** accounts for a much greater local distortion from planarity. The dihedral angle between the planes passing through the central ring and the terminal ring is 48.0°. Interestingly, however, a least-squares plane fit through the 52 cyclic C atoms gives the sum of squared atom-to-plane distances equal to 34.8 Å^2, which is only slightly larger than the value of 32.6 Å^2 calculated for the more distorted [4]helicene molecule in the crystal structure of **7**. Nevertheless, the atom-to-plane distances in molecule **8** vary in a notably greater range, from −2.375 to 2.355 Å. These observations indicate that the peripheral regions of **8** are relatively flat, which explains the similarity of the sum of least-squares deviations to that observed for the more distorted molecule in the crystal structure of **7**. This relative flatness of the peripheral regions of **8** provides for an efficient crystal packing in which molecules are arranged in layers parallel to the *ac* plane of the lattice. Within the layers, the molecules are organized in columns due to intermolecular $\pi-\pi$ interactions (Figure 9d), and the molecules from neighboring columns interact with each other via weaker $\sigma-\pi$ contacts.

Photophysical Properties. The diketones **7** and **8** are yellow powders that give greenish yellow solutions in

https://doi.org/10.1021/jacs.2c09637
J. Am. Chem. Soc. 2022, 144, 23448−23464

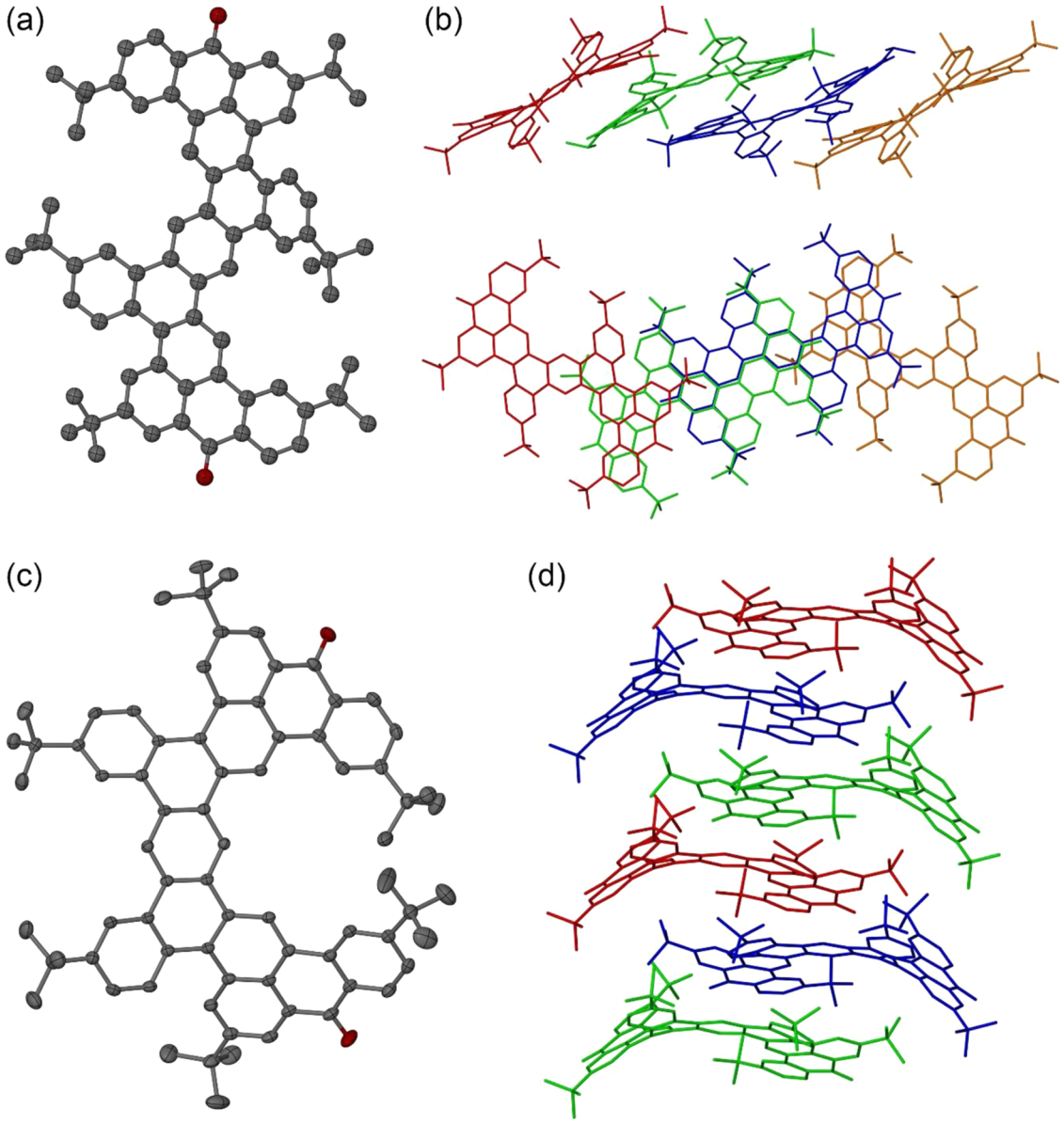

Figure 9. (a) Thermal ellipsoid plot of one of the [4]helicene molecules in the asymmetric unit of **7** and (b) side and top views of molecular chains in the crystal packing of **7**. (c) Thermal ellipsoid plot of the asymmetric unit of **8** and (d) side view of the molecular chain in the crystal packing of **8**.

dichloromethane. Both show similar absorption spectra with the lowest energy absorption peak at 456 nm. Interestingly, compound **7** has a ~2-fold greater extinction coefficient than **8** (3.1 vs 1.8 10^4 L/(mol cm) at 456 nm), presumably due to the differences in molecular symmetry. Both compounds **7** and **8** have featureless fluorescence spectra with the emission maxima at 512 and 518 nm, respectively. The two diketones are highly fluorescent with relatively high quantum yields (QY) (0.87 for **7** and 0.80 for **8**) (Figure 10).

Conversion of diketones **7** and **8** into diradicals **K** and **NK** leads to bathochromic shift in absorbance. Both compounds **K** and **NK** are red powders and give red colored solutions in dichloromethane. The two molecules show similar features in the absorption spectrum—the lowest energy peaks at 527 and 460 nm for **NK** vs 529 and 467 nm for **K**. Additionally, **K** also has two very weak absorptions at 704 and 780 nm. These two lower energy bands are similar in energy to the low-lying singlet excited states typical for singlet diradicaloids and are suggested to originate from a doubly excited electronic configuration (H,H → L,L) (H: highest occupied molecular orbital (HOMO); L: lowest unoccupied molecular orbital (LUMO)).[98] Such transitions may be another manifestation of the hidden zwitter-ionic character of singlet diradicals.[99] **NK** also shows two lower energy bands at 594 and 785 nm. These bands could be either due to doubly excited electronic configuration (H,H → L,L) or due to minor impurities (Figure 11).

The calculated spectra for the truncated versions of chromophores (with the alkyl and alkynyl substituents absent) generally agree with the experimentally measured spectra (Figure S12). There are characteristic absorbances at 500−550 nm that are observed for the **K** and **NK** cores in both the singlet and the triplet states. Interestingly, the calculated spectra for monoradicals (Figure S13) also reveal electronic transitions in this region. The calculated spectrum for singlet **K** also displays a peak at 850 nm.

https://doi.org/10.1021/jacs.2c09637
J. Am. Chem. Soc. 2022, 144, 23448−23464

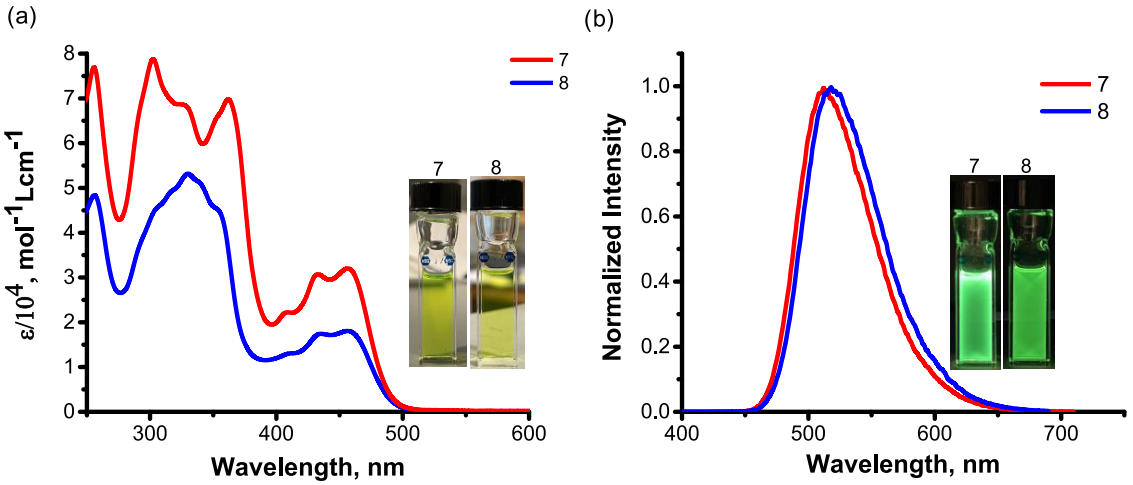

Figure 10. (a) Absorption spectra of diketones **7** and **8** in dichoromethane (pictures of **7** and in dichloromethane are shown as well). (b) Emission spectra of diketones **7** and **8** in dichloromethane (pictures of **7** and **8** under UV (365 nm) are shown as well).

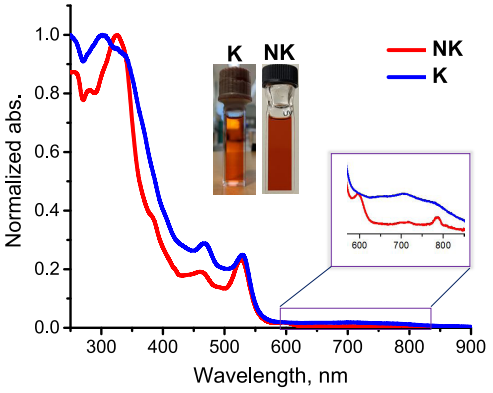

Figure 11. Absorption spectra of **K** and **NK** in dichloromethane.

Cyclic Voltammetry (CV). Cyclic voltammetry and differential pulse voltammetry measurements for both compounds **K** and **NK** (1 mg/mL) were recorded by scanning the potential from −1.4 to 0.5 V (vs Ag/Ag^{+}) at a scan rate of 0.05 V/s (Figure 12). The CVs of the two compounds recorded in DCM each exhibit two redox couples, which are electrochemically quasi-reversible as evidenced by their peak-to-peak separations (ΔE_p in Table 1). For each compound, we have named the process occurring at the more oxidizing potential as "ox" and the process occurring at the more reducing potential as "red." The values of the half-wave potentials for the two processes are $E_{1/2}^{ox} = -0.15$ V and $E_{1/2}^{red} = -1.32$ V. The DPV measurements are also consistent with CV measurements in that a peak is evident at the stated half-wave potentials.

The results of the electrochemical investigations are summarized in Table 1. The "HOMO/LUMO" energy levels of both compounds are nearly identical. They were calculated (−4.54 and −3.60 eV, respectively) from the onset potential of the oxidation (E_{ox}^{onset}) and reduction (E_{red}^{onset}) processes according to the following equations: HOMO = $-(4.8 + E_{ox}^{onset})$ eV and LUMO = $-(4.8 + E_{red}^{onset})$ eV.[100] The current crossover on the CVs for both compounds at potential <−1.5 V arises as the scan started in the diffusion-limited region. Electrochemical measurements suggest that oxidation and reduction proceed as two-electron ($E_{ox}^{1} = E_{ox}^{2}$ and $E_{red}^{1} = E_{red}^{2}$) processes rather than two one-electron processes since the one-electron Fc/Fc+ redox couple (used as the internal reference) has approximately double the peak-to-peak separation. This scenario is possible for systems with two degenerate molecular orbitals.[101] For an extended analysis of the CV data, see the SI Section.

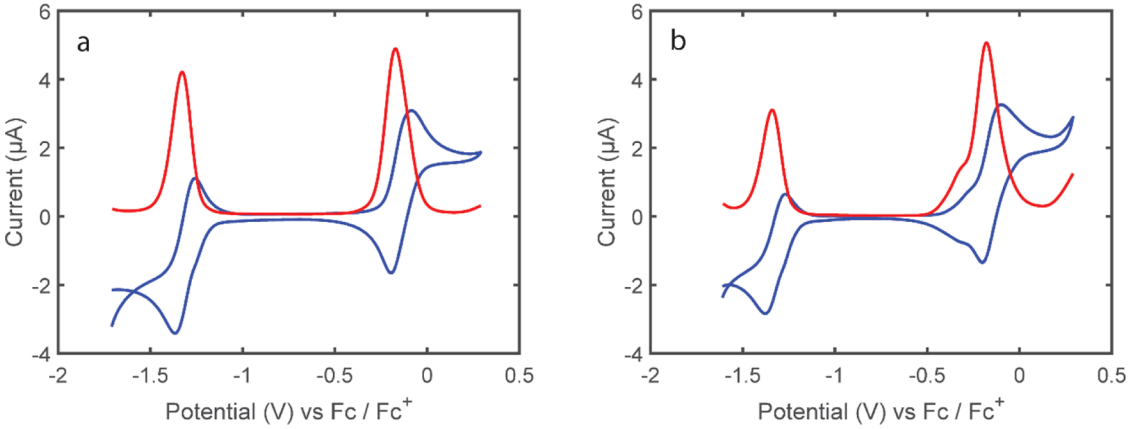

Figure 12. Cyclic voltammograms (blue) and differential pulse voltammograms (red) of compounds (a) **K** and (b) **NK** in DCM with 100 mM NBu4PF4.

https://doi.org/10.1021/jacs.2c09637
J. Am. Chem. Soc. 2022, 144, 23448−23464

Table 1. Electrochemical Parameters Determined from CVs[a]

sample	$E^{ox}_{1/2}$ (V)	$E^{red}_{1/2}$ (V)	E^{onset}_{ox} (V)	E^{onset}_{red}t (V)	ΔE_p (ox) (mV)	ΔE_p (red) (mV)	HOMO (eV)	LUMO (eV)
K	−0.15	−1.32	−0.26	−1.20	105	110.1	−4.54	−3.60
NK	−0.15	−1.32	−0.26	−1.20	109	106.8	−4.54	−3.60

[a]The onset potentials were determined using the intersection of asymptotic lines from the baseline current preceeding the redox wave and the increasing current at the fast-rising portion of the redox wave.

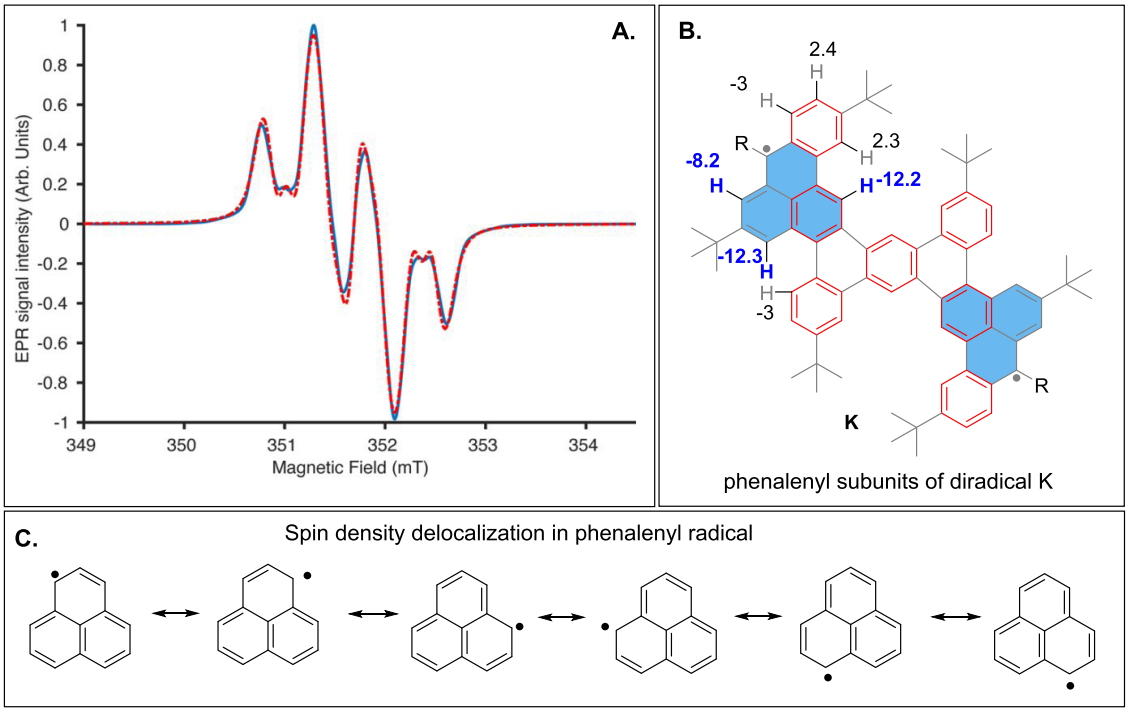

Figure 13. (A) X-band EPR spectrum (blue line) of the Kekule diradicaloid **K** recorded at room temperature and the best fit (red dotted line using EasySpin[102]) accounting for the four strongest ^{1}H hyperfine couplings. The additional hyperfine couplings have been considered as contributing to the line broadening. The analogous data for **NK** are given in the SI. (B) Core structure of the **K**-diradical and the calculated hyperfine coupling constants illustrate that spin delocalization is mostly confined to the phenalenyl subunit of the conjugated core. Large coupling constants are observed with the three H atoms in the phenalenyl subunit (bold blue). Smaller coupling constants are found for remote H atoms (shown in gray). (C) Spin density delocalization in the parent phenalenyl radical.

EPR Spectroscopy. Solution electron paramagnetic resonance (EPR) spectra of the **K** and **NK** radicals were recorded at room temperature at X-band (~9.5 GHz). The two EPR spectra appear very similar (Figure S15) and display splitting that highlights significant isotropic hyperfine couplings. Figure 13 shows the best fit of the EPR spectrum of **K**, assuming only isotropic contributions, i.e., neglecting the molecular tumbling. The fit was obtained by considering only the strongest hyperfine couplings predicted by density functional theory (DFT) (M06, def2-TZVPP basis) to avoid over-parametrization. The resulting hyperfine couplings are [15.1(2), 14.0(1), 11.1(1), 5.4(1)] MHz, in line with the DFT prediction that underestimated these values by ~20%. The overall intensity of the hyperfine couplings correlates with the predicted spin density.

Magnetic behaviors of **K** and **NK** were further probed by variable-temperature EPR spectroscopy on the powder samples of the two diradicaloids. The hyperfine structure observed in the solution EPR spectra is lost in the solid-state spectra, due to anisotropic components of the hyperfine couplings and the broadening caused by intermolecular dipolar coupling. The spectra show broad peaks with the *g*-value of 2.0026 ± 0.0001 for **K** and **NK**. The derivative EPR spectra of the two compounds show opposite trends as a function of temperature (Figure S16), but analysis of the EPR double integral reveals that this difference is the result of increased spectral broadening for **K**. Indeed, the analysis showed that the total spectral intensity (I) of the corresponding peaks increases for both compounds (Figure 14). These data, normalized by the intensity observed at the lowest experimental temperature of 100 K (I_0 at T_0), were fit to the formula

$$\frac{I}{I_0} = \frac{T_0(3 + e^{-\Delta/kT_0})}{T(3 + e^{-\Delta/kT})}$$

Derived from the Bleaney−Bowers equation, $\Delta = E_S - E_T$ is a singlet−triplet energy gap. The fitting procedure gave $\Delta = -48.0(6)$ cm^{-1}, or −0.137(2) kcal/mol, for **K**, indicating that the singlet state is lower in energy in this compound. Unfortunately, we were unable to achieve a reliable fit for **NK** due to the higher noise in the data and a limited temperature range of the solid-state EPR experiment. The best-fit value $\Delta = -18(4)$ cm^{-1} might suggest that the S−T gap becomes smaller in **NK** as compared to **K**, but satisfactory simulations of the temperature dependence of the EPR signal intensity also could be obtained with the values of Δ equal to −40 or +20 cm^{-1}, as shown in Figure 14.

https://doi.org/10.1021/jacs.2c09637
J. Am. Chem. Soc. 2022, 144, 23448−23464

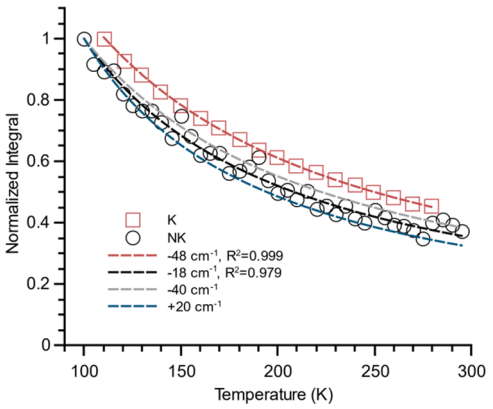

Figure 14. Evolution of the double integral of the EPR spectrum as a function of temperature for **K** (red squares) and **NK** (black circles). The double integrals were normalized with respect to the lowest temperature point. The lines correspond to the best fit using the Bleaney−Bowers equation (red for **K**, with R^2 = 0.999 and black for **NK**, with R^2 = 0.979).

Computations. To understand the singlet and triplet ground states of **K** and **NK**, respectively, we did calculations on the respective core structures. The degree of diradical character (y_0) for singlet diradicaloid **K** was estimated from the electron occupancies of frontier natural orbitals using Yamaguchi's scheme at the UCAM-B3LYP/6-31G(d,p) level of theory. The computations produced a very high y_0 value of 0.98. It was also calculated that **K** has a small S−T gap of ΔE_{S-T} = −0.3 kcal/mol, while **NK** has an equally small S−T gap of ΔE_{S-T} = +0.2 kcal/mol. Although **K** is a ground-state singlet, while **NK** is a ground-state triplet, the difference between the two states in both of these systems is very small, explaining the absence of NMR signals at room temperature. Gratifyingly, the computational data are in agreement with the experimentally measured trends in the S/T gaps for the two diradicals (i.e., 0.14 kcal/mol for **K** and an even smaller, closer to zero, gap for **NK**).

The high diradical character of **K** can be explained from the gain of additional five Clar's sextets when moving from closed-shell to open-shell configurations i.e.; two Clar's aromatic sextets in the closed-shell form to seven Clar's sextets in the open-shell form. It is also consistent with the results from NICS(1)$_{zz}$ scans.[103,104] The scan showed larger negative NICS(1)$_{zz}$ for the seven localized aromatic sextets in Figure 15a. Similar results are found for **NK** where the NICS(1)$_{zz}$ scan also shows seven localized aromatic sextets (Figure 15b). The perfect localization of the Clar's sextets is partially compromised in the vicinity of the radical centers because the delocalization of the radical is a powerful force that influences the electronic structures of the adjacent π-rings. One can think about this substructure as the phenalenyl subunit embedded into a polyaromatic framework. This observation illustrates both the power and limitations of the Clar's localized aromaticity approach to the control of the electronic structure of extended polyaromatics.

The NICS values are also consistent with the radical delocalization patterns revealed by the nature of singly occupied molecular orbitals (SOMOs) of the two diradicaloids (Figures S17 and S18) and the distribution of spin density (Figure 16). There is little radical density at central rings that correspond to the perfect Clar's subunits and at the armchair edges. In other words, we see two benzaphenalenyl radicals separated by an insulating bridge. We note that there is significant spin contamination in the singlet state of the diradicaloid **K** ($\langle S^2 \rangle$ = 1.2975), so the associated spin density in Figure 16 should be interpreted with caution. The spin density for the triplet state of this molecule is qualitatively similar (Figure S19) and is also consistent with the NICS values.

This behavior paves the way to the emergence of spin states at the zigzag edges of larger carbon nanostructures.[105−109] Overall, the spin distribution is reminiscent of two benzaphenalenyl radicals separated by a para-(**K**) or a meta-(**NK**) terphenyl moiety. It is interesting how little radical density does the terphenyl core acquire—another illustration of resilience resulting from the synergy of several Clar's sextets (Figure S5).

CONCLUSIONS

This work describes a systematic and general approach to the design of new polyaromatic diradicaloids. This approach starts with privileged aromatic core structures with the maximum number of Clar's sextets and explores the alternative electron

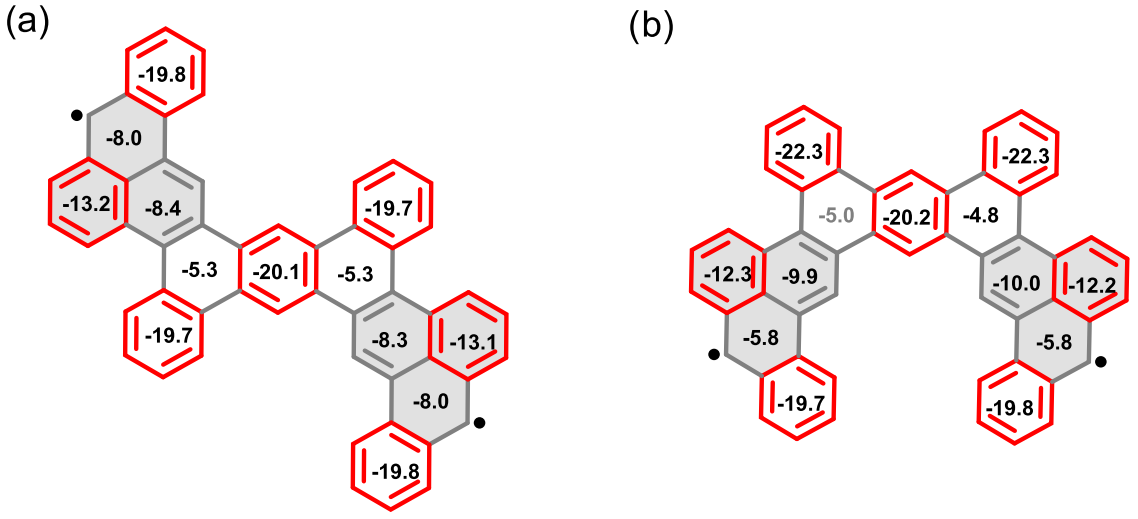

Figure 15. NICS(1) values of core structures of (a) **K** and (b) **NK**. Calculations are performed at (U)B3LYP/6-311++g(d,p) level of theory.

https://doi.org/10.1021/jacs.2c09637
J. Am. Chem. Soc. 2022, 144, 23448−23464

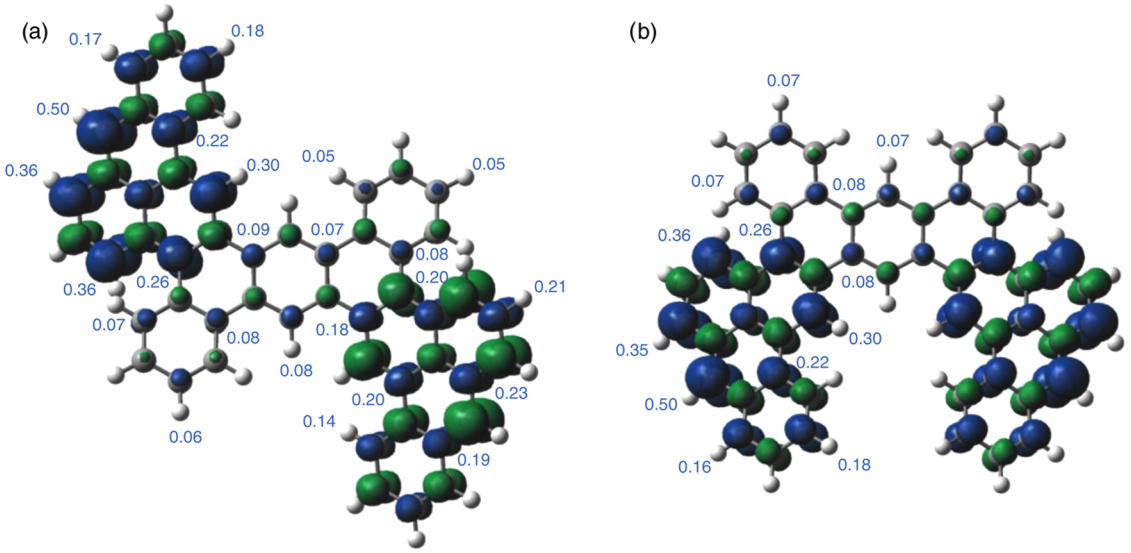

Figure 16. Spin densities for the core structures of (a) Kekulé diradicaloid **K** (singlet) and (b) non-Kekulé diradicaloid **NK** (triplet). Calculations are performed at CAM-B3LYP/6-31G(d,p) level of theory. The $\langle S^2 \rangle$ values for **K** (singlet) and **NK** (triplet) are 1.2975 and 2.2962, respectively.

pairing topologies by the addition of CH_2 radicals as spin probes at different positions at the core. Computational results clearly illustrate how, for the same core, the gain of a larger number of Clar's sextets in the open-shell form increases the diradical character parameter y_0 from 0 to 0.98 (where 1.0 indicates a perfect diradical). In this analysis, the aromatic core serves as a tunable "resistor" that is placed between the two electronic spins to prevent their coupling into a π-bond.

This theoretical analysis identified two practically accessible isomeric diradicaloid topologies, one of Kekulé (**K**) type and another of non-Kekulé (**NK**) type. **K** was calculated to have a very high diradical character of 0.98 and be a ground-state singlet with a very low singlet−triplet gap, ΔE_{ST} = −0.3 kcal/mol. **NK** was calculated to have a triplet ground state with y_0 = 1 and singlet−triplet gap, ΔE_{ST} = 0.2 kcal/mol.

We tested these theoretical predictions by synthesizing and characterizing isomeric tridecacyclic polyaromatic diradicaloids, **K** and **NK**. The two isomeric systems were assembled using a sequence of radical periannulations, cross-coupling, and C−H activation. Both molecules are NMR-inactive but EPR-active at room temperature. The diradicals are kinetically stabilized by six *tert*-butyl substituents and (triisopropylsilyl)-acetylene groups. In good agreement with the computational data, the experimentally measured hyperfine coupling constants in the EPR spectra of diradicaloids **K** and **NK** indicate that spin density is mostly confined in the individual phenalenyl units. Despite having high diradical character, both molecules were stable in inert atmosphere in the absence of light. **K** was moderately stable even in the presence of air and light, with a half-lifetime of 42 h. The non-Kekulé diradical **NK** had a shorter half-lifetime of 2 h.

In summary, this work illustrates how the theoretical design of diradicals assisted by computations and new synthetic methods (the radical periannulation) opens synthetic access to relatively stable polyaromatics with a very high diradical character. In the future, it might be of interest to explore pathways for electronic coupling and magnetic exchange across and between polyaromatic systems.[110] Such development may lead to molecules that serve as appealing building blocks for organic electronic materials.

■ ASSOCIATED CONTENT

Supporting Information

The Supporting Information is available free of charge at https://pubs.acs.org/doi/10.1021/jacs.2c09637.

Full experimental details, ^{1}H NMR and ^{13}C NMR spectra for all of the prepared compounds, X-ray crystallographic data for selected products, and computational details for all calculated structures (PDF)

Accession Codes

CCDC 2160124−2160125 contain the supplementary crystallographic data for this paper. These data can be obtained free of charge via www.ccdc.cam.ac.uk/data_request/cif, or by emailing data_request@ccdc.cam.ac.uk, or by contacting The Cambridge Crystallographic Data Centre, 12 Union Road, Cambridge CB2 1EZ, UK; fax: +44 1223 336033.

■ AUTHOR INFORMATION

Corresponding Author

Igor V. Alabugin − *Department of Chemistry and Biochemistry, Florida State University, Tallahassee, Florida 32306-4390, United States;* orcid.org/0000-0001-9289-3819; Email: alabugin@chem.fsu.edu

Authors

Febin Kuriakose − *Department of Chemistry and Biochemistry, Florida State University, Tallahassee, Florida 32306-4390, United States*

Michael Commodore − *Department of Chemistry and Biochemistry, Florida State University, Tallahassee, Florida 32306-4390, United States*

Chaowei Hu − *Department of Chemistry and Biochemistry, Florida State University, Tallahassee, Florida 32306-4390, United States;* orcid.org/0000-0002-6258-6882

Catherine J. Fabiano − *Department of Chemistry and Biochemistry, Florida State University, Tallahassee, Florida 32306-4390, United States*

Debashis Sen − *Department of Chemistry and Biochemistry, Florida State University, Tallahassee, Florida 32306-4390, United States;* orcid.org/0000-0002-8052-0019

https://doi.org/10.1021/jacs.2c09637
J. Am. Chem. Soc. 2022, 144, 23448−23464

Run R. Li − *Department of Chemistry and Biochemistry, Florida State University, Tallahassee, Florida 32306-4390, United States;* orcid.org/0000-0002-3349-3169
Shubham Bisht − *Department of Chemistry and Biochemistry, Florida State University, Tallahassee, Florida 32306-4390, United States*
Ökten Üngör − *Department of Chemistry and Biochemistry, Florida State University, Tallahassee, Florida 32306-4390, United States;* orcid.org/0000-0001-7071-6651
Xinsong Lin − *Department of Chemistry and Biochemistry, Florida State University, Tallahassee, Florida 32306-4390, United States;* orcid.org/0000-0002-0605-3029
Geoffrey F. Strouse − *Department of Chemistry and Biochemistry, Florida State University, Tallahassee, Florida 32306-4390, United States;* orcid.org/0000-0003-0841-282X
A. Eugene DePrince, III − *Department of Chemistry and Biochemistry, Florida State University, Tallahassee, Florida 32306-4390, United States;* orcid.org/0000-0003-1061-2521
Robert A. Lazenby − *Department of Chemistry and Biochemistry, Florida State University, Tallahassee, Florida 32306-4390, United States;* orcid.org/0000-0002-3622-4108
Frederic Mentink-Vigier − *National High Magnetic Field Laboratory, Florida State University, Tallahassee, Florida 32310, United States;* orcid.org/0000-0002-3570-9787
Michael Shatruk − *Department of Chemistry and Biochemistry, Florida State University, Tallahassee, Florida 32306-4390, United States*

Complete contact information is available at: https://pubs.acs.org/10.1021/jacs.2c09637

Notes

The authors declare no competing financial interest.

■ ACKNOWLEDGMENTS

The authors are grateful to the National Science Foundation for the financial support of research at FSU (awards CHE-2102579 to I.V.A. and CHE-1955754 to M.S.). The Rigaku Synergy-S single-crystal X-ray diffractometer was acquired through the NSF MRI program (award CHE-1828362). F.K. is grateful to Prof. Jack Saltiel and Dr. Sumesh Krishnan for the use of their HPLC, UV−vis, and fluorimeter instruments and to Patricia Mehaffy for the experimental assistance. F.K. and I.V.A. are grateful for helpful discussions from Prof. Jishan Wu. R.A.L. is grateful to Florida State University for start-up funds. This project also used resources at the National High Magnetic Field Laboratory supported by the National Science Foundation (DMR-1644779) and the State of Florida, as well as resources provided by the X-ray Crystallography Center (FSU075000XRAY) and the Materials Characterization Laboratory (FSU075000MAC) at the FSU Department of Chemistry and Biochemistry. The computational work was supported by the Army Research Office Small Business Technology Transfer (STTR) program under Grant No. W911NF-19-C0048.

■ REFERENCES

(1) Kamada, K.; Ohta, K.; Kubo, T.; Shimizu, A.; Morita, Y.; Nakasuji, K.; Kishi, R.; Ohta, S.; Furukawa, S.; Takahashi, H.; Nakano, M. Strong Two-Photon Absorption of Singlet Diradical Hydrocarbons. *Angew. Chem., Int. Ed.* **2007**, *46*, 3544−3546.
(2) Chikamatsu, M.; Mikami, T.; Chisaka, J.; Yoshida, Y.; Azumi, R.; Yase, K.; Shimizu, A.; Kubo, T.; Morita, Y.; Nakasuji, K. Ambipolar Organic Field-Effect Transistors Based on a Low Band Gap Semiconductor with Balanced Hole and Electron Mobilities. *Appl. Phys. Lett.* **2007**, *91*, No. 043506.
(3) Chase, D. T.; Fix, A. G.; Kang, S. J.; Rose, B. D.; Weber, C. D.; Zhong, Y.; Zakharov, L. N.; Lonergan, M. C.; Nuckolls, C.; Haley, M. M. 6,12-Diarylindeno[1,2-b]Fluorenes: Syntheses, Photophysics, and Ambipolar OFETs. *J. Am. Chem. Soc.* **2012**, *134*, 10349−10352.
(4) Lee, J.; Jadhav, P.; Reusswig, P. D.; Yost, S. R.; Thompson, N. J.; Congreve, D. N.; Hontz, E.; Van Voorhis, T.; Baldo, M. A. Singlet Exciton Fission Photovoltaics. *Acc. Chem. Res.* **2013**, *46*, 1300−1311.
(5) Son, Y.-W.; Cohen, M. L.; Louie, S. G. Energy Gaps in Graphene Nanoribbons. *Phys. Rev. Lett.* **2006**, *97*, No. 216803.
(6) Jousselin-Oba, T.; Mamada, M.; Marrot, J.; Maignan, A.; Adachi, C.; Yassar, A.; Frigoli, M. Excellent Semiconductors Based on Tetracenotetracene and Pentacenopentacene: From Stable Closed-Shell to Singlet Open-Shell. *J. Am. Chem. Soc.* **2019**, *141*, 9373−9381.
(7) Kubo, T. Syntheses and Properties of Open-Shell π-Conjugated Molecules. *Bull. Chem. Soc. Jpn.* **2021**, *94*, 2235−2244.
(8) Abe, M. Diradicals. *Chem. Rev.* **2013**, *113*, 7011−7088.
(9) Nakano, M.; Minami, T.; Yoneda, K.; Muhammad, S.; Kishi, R.; Shigeta, Y.; Kubo, T.; Rougier, L.; Champagne, B.; Kamada, K.; Ohta, K. Giant Enhancement of the Second Hyperpolarizabilities of Open-Shell Singlet Polyaromatic Diphenalenyl Diradicaloids by an External Electric Field and Donor−Acceptor Substitution. *J. Phys. Chem. Lett.* **2011**, *2*, 1094−1098.
(10) Nakano, M.; Kishi, R.; Takebe, A.; Nate, M.; Takahashi, H.; Kubo, T.; Kamada, K.; Ohta, K.; Champagne, B.; Botek, E. Second Hyperpolarizability of Zethrenes. *Comput. Lett.* **2007**, *3*, 333−338.
(11) Nakano, M.; Kishi, R.; Nakagawa, N.; Ohta, S.; Takahashi, H.; Furukawa, S.; Kamada, K.; Ohta, K.; Champagne, B.; Botek, E.; Yamada, S.; Yamaguchi, K. Second Hyperpolarizabilities (γ) of Bisimidazole and Bistriazole Benzenes: Diradical Character, Charged State, and Spin State Dependences. *J. Phys. Chem. A* **2006**, *110*, 4238−4243.
(12) Nakano, M.; Kishi, R.; Nitta, T.; Kubo, T.; Nakasuji, K.; Kamada, K.; Ohta, K.; Champagne, B.; Botek, E.; Yamaguchi, K. Second Hyperpolarizability (γ) of Singlet Diradical System: Dependence of γ on the Diradical Character. *J. Phys. Chem. A* **2005**, *109*, 885−891.
(13) Nakano, M.; Kishi, R.; Ohta, S.; Takahashi, H.; Kubo, T.; Kamada, K.; Ohta, K.; Botek, E.; Champagne, B. Relationship between Third-Order Nonlinear Optical Properties and Magnetic Interactions in Open-Shell Systems: A New Paradigm for Nonlinear Optics. *Phys. Rev. Lett.* **2007**, *99*, No. 033001.
(14) Smith, M. B.; Michl, J. Singlet Fission. *Chem. Rev.* **2010**, *110*, 6891−6936.
(15) Wen, J.; Havlas, Z.; Michl, J. Captodatively Stabilized Biradicaloids as Chromophores for Singlet Fission. *J. Am. Chem. Soc.* **2015**, *137*, 165−172.
(16) Lukman, S.; Richter, J. M.; Yang, L.; Hu, P.; Wu, J.; Greenham, N. C.; Musser, A. J. Efficient Singlet Fission and Triplet-Pair Emission in a Family of Zethrene Diradicaloids. *J. Am. Chem. Soc.* **2017**, *139*, 18376−18385.
(17) Ullrich, T.; Pinter, P.; Messelberger, J.; Haines, P.; Kaur, R.; Hansmann, M. M.; Munz, D.; Guldi, D. M. Singlet Fission in Carbene-Derived Diradicaloids. *Angew. Chem., Int. Ed.* **2020**, *59*, 7906−7914.
(18) Ullrich, T.; Munz, D.; Guldi, D. M. Unconventional Singlet Fission Materials. *Chem. Soc. Rev.* **2021**, *50*, 3485−3518.
(19) Minami, T.; Nakano, M. Diradical Character View of Singlet Fission. *J. Phys. Chem. Lett.* **2012**, *3*, 145−150.
(20) Qi, F.; Sorkhabi, O.; Suits, A. G. Evidence of Triplet Ethylene Produced from Photodissociation of Ethylene Sulfide. *J. Chem. Phys.* **2000**, *112*, 10707−10710.
(21) Hinkel, F.; Freudenberg, J.; Bunz, U. H. F. A Stable π-Conjugated Singlet Biradical. *Angew. Chem., Int. Ed.* **2016**, *55*, 9830−9832.

(22) Chen, Q.; Baumgarten, M.; Wagner, M.; Hu, Y.; Hou, I. C.-Y.; Narita, A.; Müllen, K. Dicyclopentaannelated Hexa-Peri-Hexabenzocoronenes with a Singlet Biradical Ground State. *Angew. Chem., Int. Ed.* **2021**, *60*, 11300−11304.
(23) Jones, R. R.; Bergman, R. G. P-Benzyne. Generation as an Intermediate in a Thermal Isomerization Reaction and Trapping Evidence for the 1,4-Benzenediyl Structure. *J. Am. Chem. Soc.* **1972**, *94*, 660−661.
(24) Bergman, R. G. Reactive 1,4-Dehydroaromatics. *Acc. Chem. Res.* **1973**, *6*, 25−31.
(25) Liu, J.; Ravat, P.; Wagner, M.; Baumgarten, M.; Feng, X.; Müllen, K. Tetrabenzo[a,f,j,o]Perylene: A Polycyclic Aromatic Hydrocarbon With An Open-Shell Singlet Biradical Ground State. *Angew. Chem., Int. Ed.* **2015**, *54*, 12442−12446.
(26) Dressler, J. J.; Haley, M. M. Learning How to Fine-Tune Diradical Properties by Structure Refinement. *J. Phys. Org. Chem.* **2020**, *33*, No. e4114.
(27) Rudebusch, G. E.; Zafra, J. L.; Jorner, K.; Fukuda, K.; Marshall, J. L.; Arrechea-Marcos, I.; Espejo, G. L.; Ponce Ortiz, R.; Gómez-García, C. J.; Zakharov, L. N.; Nakano, M.; Ottosson, H.; Casado, J.; Haley, M. M. Diindeno-Fusion of an Anthracene as a Design Strategy for Stable Organic Biradicals. *Nat. Chem.* **2016**, *8*, 753−759.
(28) Dressler, J. J.; Teraoka, M.; Espejo, G. L.; Kishi, R.; Takamuku, S.; Gómez-García, C. J.; Zakharov, L. N.; Nakano, M.; Casado, J.; Haley, M. M. Thiophene and Its Sulfur Inhibit Indenoindenodibenzothiophene Diradicals from Low-Energy Lying Thermal Triplets. *Nat. Chem.* **2018**, *10*, 1134−1140.
(29) Barker, J. E.; Dressler, J. J.; Cárdenas Valdivia, A.; Kishi, R.; Strand, E. T.; Zakharov, L. N.; MacMillan, S. N.; Gómez-García, C. J.; Nakano, M.; Casado, J.; Haley, M. M. Molecule Isomerism Modulates the Diradical Properties of Stable Singlet Diradicaloids. *J. Am. Chem. Soc.* **2020**, *142*, 1548−1555.
(30) Frederickson, C. K.; Rose, B. D.; Haley, M. M. Explorations of the Indenofluorenes and Expanded Quinoidal Analogues. *Acc. Chem. Res.* **2017**, *50*, 977−987.
(31) Hayashi, H.; Barker, J. E.; Cárdenas Valdivia, A.; Kishi, R.; MacMillan, S. N.; Gómez-García, C. J.; Miyauchi, H.; Nakamura, Y.; Nakano, M.; Kato, S.; Haley, M. M.; Casado, J. Monoradicals and Diradicals of Dibenzofluoreno[3,2-b]Fluorene Isomers: Mechanisms of Electronic Delocalization. *J. Am. Chem. Soc.* **2020**, *142*, 20444−20455.
(32) Frederickson, C. K.; Zakharov, L. N.; Haley, M. M. Modulating Paratropicity Strength in Diareno-Fused Antiaromatics. *J. Am. Chem. Soc.* **2016**, *138*, 16827−16838.
(33) Clar, E.*Polycyclic Hydrocarbons*; Academic Press: London, 1964.
(34) Clar, E.*The Aromatic Sextet*; Wiley: NewYork, NY, 1972.
(35) Clar, E.; Zander, M. 378. 1: 12-2: 3-10: 11-Tribenzoperylene. *J. Chem. Soc. (Resumed)* **1958**, 1861−1865.
(36) Zeng, Z.; Shi, X.; Chi, C.; Navarrete, J. T. L.; Casado, J.; Wu, J. Pro-Aromatic and Anti-Aromatic π-Conjugated Molecules: An Irresistible Wish to Be Diradicals. *Chem. Soc. Rev.* **2015**, *44*, 6578−6596.
(37) Stuyver, T.; Chen, B.; Zeng, T.; Geerlings, P.; De Proft, F.; Hoffmann, R. Do Diradicals Behave Like Radicals? *Chem. Rev.* **2019**, *119*, 11291−11351.
(38) Konishi, A.; Hirao, Y.; Nakano, M.; Shimizu, A.; Botek, E.; Champagne, B.; Shiomi, D.; Sato, K.; Takui, T.; Matsumoto, K.; Kurata, H.; Kubo, T. Synthesis and Characterization of Teranthene: A Singlet Biradical Polycyclic Aromatic Hydrocarbon Having Kekulé Structures. *J. Am. Chem. Soc.* **2010**, *132*, 11021−11023.
(39) Konishi, A.; Hirao, Y.; Matsumoto, K.; Kurata, H.; Kishi, R.; Shigeta, Y.; Nakano, M.; Tokunaga, K.; Kamada, K.; Kubo, T. Synthesis and Characterization of Quarteranthene: Elucidating the Characteristics of the Edge State of Graphene Nanoribbons at the Molecular Level. *J. Am. Chem. Soc.* **2013**, *135*, 1430−1437.
(40) Ajayakumar, M. R.; Fu, Y.; Ma, J.; Hennersdorf, F.; Komber, H.; Weigand, J. J.; Alfonsov, A.; Popov, A. A.; Berger, R.; Liu, J.; Müllen, K.; Feng, X. Toward Full Zigzag-Edged Nanographenes: Peri-Tetracene and Its Corresponding Circumanthracene. *J. Am. Chem. Soc.* **2018**, *140*, 6240−6244.
(41) Zöphel, L.; Berger, R.; Gao, P.; Enkelmann, V.; Baumgarten, M.; Wagner, M.; Müllen, K. Toward the Peri-Pentacene Framework. *Chem.—Eur. J.* **2013**, *19*, 17821−17826.
(42) Ajayakumar, M. R.; Ma, J.; Lucotti, A.; Schellhammer, K. S.; Serra, G.; Dmitrieva, E.; Rosenkranz, M.; Komber, H.; Liu, J.; Ortmann, F.; Tommasini, M.; Feng, X. Persistent Peri-Heptacene: Synthesis and In Situ Characterization. *Angew. Chem., Int. Ed.* **2021**, *60*, 13853−13858.
(43) Ohashi, K.; Kubo, T.; Masui, T.; Yamamoto, K.; Nakasuji, K.; Takui, T.; Kai, Y.; Murata, I. 4,8,12,16-Tetra-Tert-Butyl-s-Indaceno-[1,2,3-Cd:5,6,7-c′d′]Diphenalene: A Four-Stage Amphoteric Redox System. *J. Am. Chem. Soc.* **1998**, *120*, 2018−2027.
(44) Kubo, T.; Sakamoto, M.; Akabane, M.; Fujiwara, Y.; Yamamoto, K.; Akita, M.; Inoue, K.; Takui, T.; Nakasuji, K. Four-Stage Amphoteric Redox Properties and Biradicaloid Character of Tetra-Tert-Butyldicyclopenta[b;d]Thieno[1,2,3-Cd;5,6,7-C′d′]-Diphenalene. *Angew. Chem., Int. Ed.* **2004**, *43*, 6474−6479.
(45) Shimizu, A.; Kubo, T.; Uruichi, M.; Yakushi, K.; Nakano, M.; Shiomi, D.; Sato, K.; Takui, T.; Hirao, Y.; Matsumoto, K.; Kurata, H.; Morita, Y.; Nakasuji, K. Alternating Covalent Bonding Interactions in a One-Dimensional Chain of a Phenalenyl-Based Singlet Biradical Molecule Having Kekulé Structures. *J. Am. Chem. Soc.* **2010**, *132*, 14421−14428.
(46) Sun, Z.; Huang, K.-W.; Wu, J. Soluble and Stable Heptazethrenebis(Dicarboximide) with a Singlet Open-Shell Ground State. *J. Am. Chem. Soc.* **2011**, *133*, 11896−11899.
(47) Li, Y.; Heng, W.-K.; Lee, B. S.; Aratani, N.; Zafra, J. L.; Bao, N.; Lee, R.; Sung, Y. M.; Sun, Z.; Huang, K.-W.; Webster, R. D.; López Navarrete, J. T.; Kim, D.; Osuka, A.; Casado, J.; Ding, J.; Wu, J. Kinetically Blocked Stable Heptazethrene and Octazethrene: Closed-Shell or Open-Shell in the Ground State? *J. Am. Chem. Soc.* **2012**, *134*, 14913−14922.
(48) Sun, Z.; Lee, S.; Park, K. H.; Zhu, X.; Zhang, W.; Zheng, B.; Hu, P.; Zeng, Z.; Das, S.; Li, Y.; Chi, C.; Li, R.-W.; Huang, K.-W.; Ding, J.; Kim, D.; Wu, J. Dibenzoheptazethrene Isomers with Different Biradical Characters: An Exercise of Clar's Aromatic Sextet Rule in Singlet Biradicaloids. *J. Am. Chem. Soc.* **2013**, *135*, 18229−18236.
(49) Huang, R.; Phan, H.; Herng, T. S.; Hu, P.; Zeng, W.; Dong, S.; Das, S.; Shen, Y.; Ding, J.; Casanova, D.; Wu, J. Higher Order π-Conjugated Polycyclic Hydrocarbons with Open-Shell Singlet Ground State: Nonazethrene versus Nonacene. *J. Am. Chem. Soc.* **2016**, *138*, 10323−10330.
(50) Zeng, Z.; Sung, Y. M.; Bao, N.; Tan, D.; Lee, R.; Zafra, J. L.; Lee, B. S.; Ishida, M.; Ding, J.; López Navarrete, J. T.; Li, Y.; Zeng, W.; Kim, D.; Huang, K.-W.; Webster, R. D.; Casado, J.; Wu, J. Stable Tetrabenzo-Chichibabin's Hydrocarbons: Tunable Ground State and Unusual Transition between Their Closed-Shell and Open-Shell Resonance Forms. *J. Am. Chem. Soc.* **2012**, *134*, 14513−14525.
(51) Zeng, W.; Qi, Q.; Wu, J. Toward Long Rylene Ribbons and Quinoidal Rylene Diradicaloids. *Eur. J. Org. Chem.* **2018**, *2018*, 7−17.
(52) Zeng, W.; Phan, H.; Herng, T. S.; Gopalakrishna, T. Y.; Aratani, N.; Zeng, Z.; Yamada, H.; Ding, J.; Wu, J. Rylene Ribbons with Unusual Diradical Character. *Chem* **2017**, *2*, 81−92.
(53) Doehnert, D.; Koutecky, J. Occupation Numbers of Natural Orbitals as a Criterion for Biradical Character. Different Kinds of Biradicals. *J. Am. Chem. Soc.* **1980**, *102*, 1789−1796.
(54) Yamaguchi, K.; Kawakami, T.; Takano, Y.; Kitagawa, Y.; Yamashita, Y.; Fujita, H. Analytical and Ab Initio Studies of Effective Exchange Interactions, Polyradical Character, Unpaired Electron Density, and Information Entropy in Radical Clusters (R)N: Allyl Radical Cluster (N = 2−10) and Hydrogen Radical Cluster (N = 50). *Int. J. Quantum Chem.* **2002**, *90*, 370−385.
(55) Shen, J.-J.; Han, Y.; Dong, S.; Phan, H.; Herng, T. S.; Xu, T.; Ding, J.; Chi, C. A Stable [4,3]Peri-Acene Diradicaloid: Synthesis, Structure, and Electronic Properties. *Angew. Chem., Int. Ed.* **2021**, *60*, 4464−4469.

https://doi.org/10.1021/jacs.2c09637
J. Am. Chem. Soc. 2022, 144, 23448−23464

(56) Solà, M. Forty Years of Clar's Aromatic π-Sextet Rule. *Front. Chem.* **2013**, *1*, No. 22.
(57) Ravat, P.; Baumgarten, M. "Tschitschibabin Type Biradicals": Benzenoid or Quinoid? *Phys. Chem. Chem. Phys.* **2015**, *17*, 983−991.
(58) Clar, E.; Stewart, D. G. Aromatic Hydrocarbons. LXV. Triangulene Derivatives1. *J. Am. Chem. Soc.* **1953**, *75*, 2667−2672.
(59) Clar, E.; Stewart, D. G. Aromatic Hydrocarbons. LXVIII. Triangulene Derivatives. Part II1. *J. Am. Chem. Soc.* **1954**, *76*, 3504−3507.
(60) Inoue, J.; Fukui, K.; Kubo, T.; Nakazawa, S.; Sato, K.; Shiomi, D.; Morita, Y.; Yamamoto, K.; Takui, T.; Nakasuji, K. The First Detection of a Clar's Hydrocarbon, 2,6,10-Tri-Tert-Butyltriangulene: A Ground-State Triplet of Non-Kekulé Polynuclear Benzenoid Hydrocarbon. *J. Am. Chem. Soc.* **2001**, *123*, 12702−12703.
(61) Pavliček, N.; Mistry, A.; Majzik, Z.; Moll, N.; Meyer, G.; Fox, D. J.; Gross, L. Synthesis and Characterization of Triangulene. *Nat. Nanotechnol.* **2017**, *12*, 308−311.
(62) Arikawa, S.; Shimizu, A.; Shiomi, D.; Sato, K.; Shintani, R. Synthesis and Isolation of a Kinetically Stabilized Crystalline Triangulene. *J. Am. Chem. Soc.* **2021**, *143*, 19599−19605.
(63) Li, Y.; Huang, K.-W.; Sun, Z.; Webster, R. D.; Zeng, Z.; Zeng, W.; Chi, C.; Furukawa, K.; Wu, J. A Kinetically Blocked 1,14:11,12-Dibenzopentacene: A Persistent Triplet Diradical of a Non-Kekulé Polycyclic Benzenoid Hydrocarbon. *Chem. Sci.* **2014**, *5*, 1908−1914.
(64) Valenta, L.; Mayländer, M.; Kappeler, P.; Blacque, O.; Šolomek, T.; Richert, S.; Juríček, M. Trimesityltriangulene: A Persistent Derivative of Clar's Hydrocarbon. *Chem. Commun.* **2022**, *58*, 3019−3022.
(65) Wei, H.; Hou, X.; Xu, T.; Zou, Y.; Li, G.; Wu, S.; Geng, Y.; Wu, J. Solution-Phase Synthesis and Isolation of An Aza-Triangulene and Its Cation in Crystalline Form. *Angew. Chem., Int. Ed.* **2022**, *61*, No. e202210386.
(66) Zhang, H.; Pink, M.; Wang, Y.; Rajca, S.; Rajca, A. High-Spin *S* = 3/2 Ground-State Aminyl Triradicals: Toward High-Spin Oligo-Aza Nanographenes. *J. Am. Chem. Soc.* **2022**, *144*, 19576−19591.
(67) Koga, Y.; Kaneda, T.; Saito, Y.; Murakami, K.; Itami, K. Synthesis of Partially and Fully Fused Polyaromatics by Annulative Chlorophenylene Dimerization. *Science* **2018**, *359*, 435−439.
(68) Ito, H.; Ozaki, K.; Itami, K. Annulative π-Extension (APEX): Rapid Access to Fused Arenes, Heteroarenes, and Nanographenes. *Angew. Chem., Int. Ed.* **2017**, *56*, 11144−11164.
(69) Krzeszewski, M.; Ito, H.; Itami, K. Infinitene: A Helically Twisted Figure-Eight [12]Circulene Topoisomer. *J. Am. Chem. Soc.* **2022**, *144*, 862−871.
(70) Scott, L. T.; Boorum, M. M.; McMahon, B. J.; Hagen, S.; Mack, J.; Blank, J.; Wegner, H.; de Meijere, A. A Rational Chemical Synthesis of C60. *Science* **2002**, *295*, 1500−1503.
(71) Scott, L. T. Methods for the Chemical Synthesis of Carbon Nanotubes: An Approach Based on Hemispherical Polyarene Templates. *Pure Appl. Chem.* **2017**, *89*, 809−820.
(72) Scott, L. T.; Hashemi, M. M.; Meyer, D. T.; Warren, H. B. Corannulene. A Convenient New Synthesis. *J. Am. Chem. Soc.* **1991**, *113*, 7082−7084.
(73) Zhao, L.; Prendergast, M. B.; Kaiser, R. I.; Xu, B.; Ablikim, U.; Ahmed, M.; Sun, B.-J.; Chen, Y.-L.; Chang, A. H. H.; Mohamed, R. K.; Fischer, F. R. Synthesis of Polycyclic Aromatic Hydrocarbons by Phenyl Addition−Dehydrocyclization: The Third Way. *Angew. Chem., Int. Ed.* **2019**, *58*, 17442−17450.
(74) Blackwell, R. E.; Zhao, F.; Brooks, E.; Zhu, J.; Piskun, I.; Wang, S.; Delgado, A.; Lee, Y.-L.; Louie, S. G.; Fischer, F. R. Spin Splitting of Dopant Edge State in Magnetic Zigzag Graphene Nanoribbons. *Nature* **2021**, *600*, 647−652.
(75) Haley, M. M.; Tykwinski, R. R.*Carbon-Rich Compounds: From Molecules to Materials*; John Wiley & Sons, 2006.
(76) Kilde, M. D.; Murray, A. H.; Andersen, C. L.; Storm, F. E.; Schmidt, K.; Kadziola, A.; Mikkelsen, K. V.; Hampel, F.; Hammerich, O.; Tykwinski, R. R.; Nielsen, M. B. Synthesis of Radiaannulene Oligomers to Model the Elusive Carbon Allotrope 6,6,12-Graphyne. *Nat. Commun.* **2019**, *10*, No. 3714.
(77) Tykwinski, R. R. Synthesis of Unsymmetrical Derivatives of Pentacene for Materials Applications. *Acc. Chem. Res.* **2019**, *52*, 2056−2069.
(78) Chalifoux, W. A.; Tykwinski, R. R. Synthesis of Polyynes to Model the Sp-Carbon Allotrope Carbyne. *Nat. Chem.* **2010**, *2*, 967−971.
(79) Yang, W.; Lucotti, A.; Tommasini, M.; Chalifoux, W. A. Bottom-Up Synthesis of Soluble and Narrow Graphene Nanoribbons Using Alkyne Benzannulations. *J. Am. Chem. Soc.* **2016**, *138*, 9137−9144.
(80) Senese, A. D.; Chalifoux, W. A. Nanographene and Graphene Nanoribbon Synthesis via Alkyne Benzannulations. *Molecules* **2019**, *24*, No. 118.
(81) Alabugin, I. V.; Gonzalez-Rodriguez, E. Alkyne Origami: Folding Oligoalkynes into Polyaromatics. *Acc. Chem. Res.* **2018**, *51*, 1206−1219.
(82) Haley, M. M. Synthesis and properties of annulenic subunits of graphyne and graphdiyne nanoarchitectures. *Pure Appl. Chem.* **2008**, *80*, 519−532.
(83) Barker, J. E.; Price, T. W.; Karas, L. J.; Kishi, R.; MacMillan, S. N.; Zakharov, L. N.; Gómez-García, C. J.; Wu, J. I.; Nakano, M.; Haley, M. M. A Tale of Two Isomers: Enhanced Antiaromaticity/Diradical Character versus Deleterious Ring-Opening of Benzofuran-Fused s-Indacenes and Dicyclopenta[b,g]Naphthalenes. *Angew. Chem., Int. Ed.* **2021**, *60*, 22385−22392.
(84) Baumgartner, T. Insights on the Design and Electron-Acceptor Properties of Conjugated Organophosphorus Materials. *Acc. Chem. Res.* **2014**, *47*, 1613−1622.
(85) Lovell, T. C.; Garrison, Z. R.; Jasti, R. Synthesis, Characterization, and Computational Investigation of Bright Orange-Emitting Benzothiadiazole [10]Cycloparaphenylene. *Angew. Chem.* **2020**, *132*, 14469−14473.
(86) Chen, Z.; Mercer, J. A. M.; Zhu, X.; Romaniuk, J. A. H.; Pfattner, R.; Cegelski, L.; Martinez, T. J.; Burns, N. Z.; Xia, Y. Mechanochemical Unzipping of Insulating Polyladderene to Semiconducting Polyacetylene. *Science* **2017**, *357*, 475−479.
(87) Jin, Z.; Teo, Y. C.; Teat, S. J.; Xia, Y. Regioselective Synthesis of [3]Naphthylenes and Tuning of Their Antiaromaticity. *J. Am. Chem. Soc.* **2017**, *139*, 15933−15939.
(88) Bergman, H. M.; Kiel, G. R.; Handford, R. C.; Liu, Y.; Tilley, T. D. Scalable, Divergent Synthesis of a High Aspect Ratio Carbon Nanobelt. *J. Am. Chem. Soc.* **2021**, *143*, 8619−8624.
(89) Lungerich, D.; Papaianina, O.; Feofanov, M.; Liu, J.; Devarajulu, M.; Troyanov, S. I.; Maier, S.; Amsharov, K. Dehydrative π-Extension to Nanographenes with Zig-Zag Edges. *Nat. Commun.* **2018**, *9*, No. 4756.
(90) Che, S.; Li, C.; Wang, C.; Zaheer, W.; Ji, X.; Phillips, B.; Gurbandurdyyev, G.; Glynn, J.; Guo, Z.-H.; Al-Hashimi, M.; Zhou, H.-C.; Banerjee, S.; Fang, L. Solution-Processable Porous Graphitic Carbon from Bottom-up Synthesis and Low-Temperature Graphitization. *Chem. Sci.* **2021**, *12*, 8438−8444.
(91) Müller, M.; Kübel, C.; Müllen, K. Giant Polycyclic Aromatic Hydrocarbons. *Chem.—Eur. J.* **1998**, *4*, 2099−2109.
(92) Cai, J.; Ruffieux, P.; Jaafar, R.; Bieri, M.; Braun, T.; Blankenburg, S.; Muoth, M.; Seitsonen, A. P.; Saleh, M.; Feng, X.; Müllen, K.; Fasel, R. Atomically Precise Bottom-up Fabrication of Graphene Nanoribbons. *Nature* **2010**, *466*, 470−473.
(93) Spisak, S. N.; Zhou, Z.; Liu, S.; Xu, Q.; Wei, Z.; Kato, K.; Segawa, Y.; Itami, K.; Rogachev, A. Y.; Petrukhina, M. A. Stepwise Generation of Mono-, Di-, and Triply-Reduced Warped Nanographenes: Charge-Dependent Aromaticity, Surface Nonequivalence, Swing Distortion, and Metal Binding Sites. *Angew. Chem., Int. Ed.* **2021**, *60*, 25445−25453.
(94) Moreno, C.; Vilas-Varela, M.; Kretz, B.; Garcia-Lekue, A.; Costache, M. V.; Paradinas, M.; Panighel, M.; Ceballos, G.; Valenzuela, S. O.; Peña, D.; Mugarza, A. Bottom-up Synthesis of Multifunctional Nanoporous Graphene. *Science* **2018**, *360*, 199−203.
(95) Tsvetkov, N. P.; Gonzalez-Rodriguez, E.; Hughes, A.; dosPassosGomes, G.; White, F. D.; Kuriakose, F.; Alabugin, I. V.

Radical Alkyne Peri-Annulation Reactions for the Synthesis of Functionalized Phenalenes, Benzanthrenes, and Olympicene. *Angew. Chem., Int. Ed.* **2018**, *57*, 3651−3655.
(96) Gonzalez-Rodriguez, E.; Abdo, M. A.; dos Passos Gomes, G.; Ayad, S.; White, F. D.; Tsvetkov, N. P.; Hanson, K.; Alabugin, I. V. Twofold π-Extension of Polyarenes via Double and Triple Radical Alkyne Peri-Annulations: Radical Cascades Converging on the Same Aromatic Core. *J. Am. Chem. Soc.* **2020**, *142*, 8352−8366.
(97) Hughes, A. M.; dos Passos Gomes, G.; Alabugin, I. V. Stereoelectronic Influence of a "Spectator" Propargylic Substituent Can Override Aromaticity Effects in Radical Peri-Cyclizations En Route to Expanded Polyaromatics. *J. Org. Chem.* **2019**, *84*, 1853−1862.
(98) Di Motta, S.; Negri, F.; Fazzi, D.; Castiglioni, C.; Canesi, E. V. Biradicaloid and Polyenic Character of Quinoidal Oligothiophenes Revealed by the Presence of a Low-Lying Double-Exciton State. *J. Phys. Chem. Lett.* **2010**, *1*, 3334−3339.
(99) Peterson, P. W.; Mohamed, R. K.; Alabugin, I. V. How to Lose a Bond in Two Ways —— The Diradical/Zwitterion Dichotomy in Cycloaromatization Reactions. *Eur. J. Org. Chem.* **2013**, *2013*, 2505−2527.
(100) Zeng, W.; Gopalakrishna, T. Y.; Phan, H.; Tanaka, T.; Herng, T. S.; Ding, J.; Osuka, A.; Wu, J. Superoctazethrene: An Open-Shell Graphene-like Molecule Possessing Large Diradical Character but Still with Reasonable Stability. *J. Am. Chem. Soc.* **2018**, *140*, 14054.
(101) Arikawa, S.; Shimizu, A.; Shiomi, D.; Sato, K.; Shintani, R. Synthesis and Isolation of a Kinetically Stabilized Crystalline Triangulene. *J. Am. Chem. Soc.* **2021**, *143*, 19599.
(102) Stoll, S.; Schweiger, A. EasySpin, a Comprehensive Software Package for Spectral Simulation and Analysis in EPR. *J. Magn. Reson.* **2006**, *178*, 42−55.
(103) Schleyer, P. v. R.; Maerker, C.; Dransfeld, A.; Jiao, H.; van Eikema Hommes, N. J. R. Nucleus-Independent Chemical Shifts: A Simple and Efficient Aromaticity Probe. *J. Am. Chem. Soc.* **1996**, *118*, 6317−6318.
(104) Chen, Z.; Wannere, C. S.; Corminboeuf, C.; Puchta, R.; Schleyer, P. v. R. Nucleus-Independent Chemical Shifts (NICS) as an Aromaticity Criterion. *Chem. Rev.* **2005**, *105*, 3842−3888.
(105) Nakada, K.; Fujita, M.; Dresselhaus, G.; Dresselhaus, M. S. Edge State in Graphene Ribbons: Nanometer Size Effect and Edge Shape Dependence. *Phys. Rev. B* **1996**, *54*, 17954−17961.
(106) Wakabayashi, K.; Fujita, M.; Ajiki, H.; Sigrist, M. Electronic and Magnetic Properties of Nanographite Ribbons. *Phys. Rev. B* **1999**, *59*, 8271−8282.
(107) Yazyev, O. V. Emergence of Magnetism in Graphene Materials and Nanostructures. *Rep. Prog. Phys.* **2010**, *73*, No. 056501.
(108) Son, Y.-W.; Cohen, M. L.; Louie, S. G. Half-Metallic Graphene Nanoribbons. *Nature* **2006**, *444*, 347−349.
(109) Kimouche, A.; Ervasti, M. M.; Drost, R.; Halonen, S.; Harju, A.; Joensuu, P. M.; Sainio, J.; Liljeroth, P. Ultra-Narrow Metallic Armchair Graphene Nanoribbons. *Nat. Commun.* **2015**, *6*, No. 10177.
(110) Ravat, P.; Šolomek, T.; Häussinger, D.; Blacque, O.; Juríček, M. Dimethylcethrene: A Chiroptical Diradicaloid Photoswitch. *J. Am. Chem. Soc.* **2018**, *140*, 10839−10847.

https://doi.org/10.1021/jacs.2c09637
J. Am. Chem. Soc. 2022, 144, 23448−23464